iScience

CellPress
OPEN ACCESS

Article

MEK-inhibitors decrease Nfix in muscular dystrophy but induce unexpected calcifications, partially rescued with Cyanidin diet

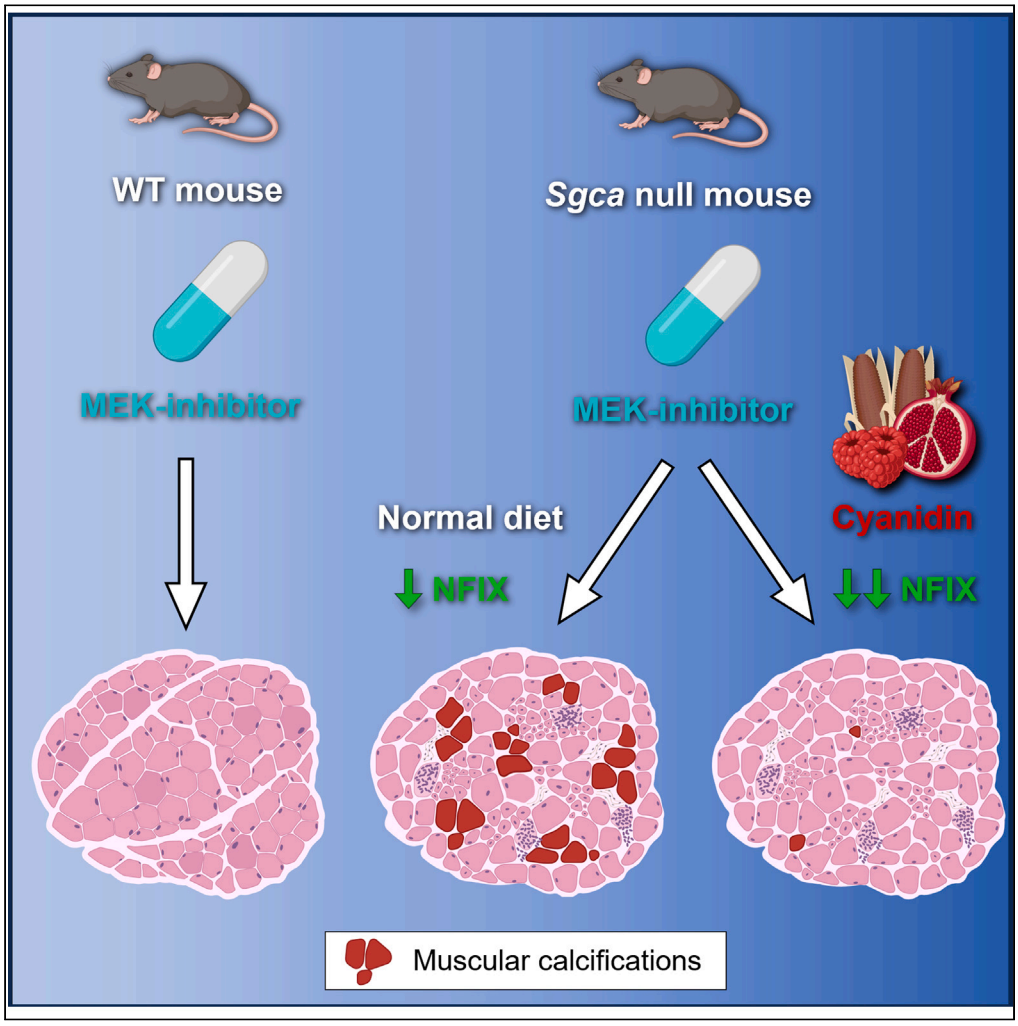

Giuseppe Angelini, Emanuele Capra, Francesca Rossi, ..., Giorgia Careccia, Chiara Bonfanti, Graziella Messina

graziella.messina@unimi.it

Highlights

MEK inhibitor decreases the Nfix protein in murine myoblasts *in vitro*

Chronic treatment with Trametinib decreases Nfix in dystrophic muscles *in vivo*

MEK inhibitors cause muscular calcifications in dystrophic muscles

Cyanidin supplementation partly rescues Trametinib-induced calcifications

Angelini et al., iScience *27*, 108696
January 19, 2024
https://doi.org/10.1016/j.isci.2023.108696

iScience

CellPress
OPEN ACCESS

Article

MEK-inhibitors decrease Nfix in muscular dystrophy but induce unexpected calcifications, partially rescued with Cyanidin diet

Giuseppe Angelini,[1] Emanuele Capra,[1,2] Francesca Rossi,[1,3] Giada Mura,[1,4] Marielle Saclier,[1,5] Valentina Taglietti,[1,6] Gabriele Rovetta,[1] Raffaele Epis,[1] Giorgia Careccia,[1] Chiara Bonfanti,[1] and Graziella Messina[1,7,*]

SUMMARY

Muscular dystrophies (MDs) are incurable genetic myopathies characterized by progressive degeneration of skeletal muscles. Dystrophic mice lacking the transcription factor Nfix display morphological and functional improvements of the disease. Recently, we demonstrated that MAPK signaling pathway positively regulates Nfix in muscle development and that Cyanidin, a natural antioxidant molecule, strongly ameliorates the pathology. To explore a synergistic approach aimed at treating MDs, we administered Trametinib, a clinically approved MEK inhibitor, alone or combined with Cyanidin to adult *Sgca* null mice. We observed that chronic treatment with Trametinib and Cyanidin reduced Nfix in myogenic cells but, unexpectedly, caused ectopic calcifications exclusively in dystrophic muscles. The combined treatment with Cyanidin resulted in histological improvements by preventing Trametinib-induced calcifications in Diaphragm and Soleus. Collectively, this first pilot study revealed that Nfix is modulated by the MAPK pathway in MDs, and that Cyanidin partly rescued the unexpected ectopic calcifications caused by MEK inhibition.

INTRODUCTION

Muscular dystrophies (MDs) are a group of inherited diseases affecting skeletal muscles. They are mainly characterized by different genetic mutations affecting the expression of proteins belonging to the dystrophin glycoprotein complex (DGC), which provides a physical support to muscle contraction. Dystrophic myofibers are highly fragile upon contraction, leading to muscular necrosis, chronic inflammation, impairments in tissue regeneration driven by the muscular stem cells or satellite cells (MuSCs), and progressive wasting of muscle tissue.[1]

Besides its mechanical function, DGC also plays an important role in the modulation of intracellular signaling pathways. Several data demonstrate that mutations in this complex impair different molecular signaling pathways underlying proliferation, differentiation, oxidative metabolism, and apoptosis of muscle cells.[2,3]

Currently approved therapies for MDs, such as those which attenuate the inflammation, are not curative but mostly slow down the disease progression although eliciting serious side effects.[4] Innovative gene therapies are targeting the MDs' causative mutations by approaches of gene correction or replacement.[5] However, the timing of treatment and the quality of muscular tissue are two crucial aspects that mostly affect the therapeutic outcomes.[6]

Nuclear factor-1X (Nfix) is a transcription factor belonging to the nuclear factor-1 (NFI) protein family with a key role in the skeletal muscle development,[7] modulating the switch from embryonic to fetal myoblasts by its conserved double-activity as activator of fetal genes and repressor of embryonic genes.[8,9] It also has a detrimental role in the progression of MDs in mice and its inhibition might be a novel therapeutic approach for these pathologies. Indeed, dystrophic muscles lacking *Nfix* display morphological and functional improvements of the disease thanks to a delay in the dystrophic cycle of muscle regeneration/degeneration, a switch toward more oxidative phenotype of myofibers, and a fine-tuning of the inflammatory process.[10–12] Furthermore, we proved that Nfix is positively regulated by the MAPK (MEK/ERK) pathway in fetal and post-natal myoblasts. Indeed, treatment with an MEK inhibitor (PD98059) causes a strong decrease in the Nfix protein levels both in murine fetal muscles *in vivo* and in postnatal MuSC-derived myoblasts *in vitro*.[13]

[1]Department of Biosciences, University of Milan, 20133 Milan, Italy
[2]Present address: Fondazione Human Technopole, 20157 Milan Italy
[3]Present address: Institute of Neurosciences, CNR, Milan, 20854, Italy
[4]Present address: Stem Cells and Development Unit, UMR3738, CNRS, Institut Pasteur, Paris, 75015, France
[5]Present address: Department of Developmental and Stem Cell Biology, UMR3738, CNRS, Institut Pasteur, Paris, 75015, France
[6]Present address: IMRB, INSERM, University of Paris Est Creteil, Creteil, 94010, France
[7]Lead contact
*Correspondence: graziella.messina@unimi.it
https://doi.org/10.1016/j.isci.2023.108696

Considering all these findings, we evaluated the effect of MEK inhibition in a dystrophic context to elucidate if this pharmaceutical approach may be beneficial for the dystrophic disease progression through the inhibition of Nfix.

To enhance the translation potential of our study, we used Trametinib (GSK1120212 or Mekinist), an allosteric, ATP noncompetitive inhibitor of MEK1/2, that shares the same molecular mechanism of PD98059 but has better pharmacological features for preclinical studies and clinical trials.[14,15] Indeed, Trametinib was approved by FDA and EMA for the treatment of metastatic melanoma, and it is currently used in clinic (NCT01682083, EMEA/H/C/002643).[16] Moreover, several studies confirmed the inability of this MEK inhibitor to target the brain (where Nfix has a crucial function in regulating the differentiation of neuronal stem cells), making these drugs suited for a pharmacological repurposing in MDs.[17–19]

As a proper animal model for MDs, we chose the *α-sarcoglycan (Sgca)* null mouse, in which the main dystrophic hallmarks (necrotic fibers, inflammation, fibrotic deposits, functional deficits) already occur at 8 days of age in both Diaphragm and at lower extent in limb muscles, hence recapitulating better the human pathology than other mouse models.[20,21]

Furthermore, to verify a synergistic effect on muscle histology, we administered Trametinib to adult *Sgca* null mice,[20] alone or in combination with Cyanidin-3-glucoside (here referred to as "Cyanidin"), the most common natural anthocyanin in red fruits.[22] Thanks to its antioxidant and anti-inflammatory properties, Cyanidin dietary intake was proved by our group to alleviate pathogenic hallmarks in dystrophic muscles, significantly reducing muscular fibrotic deposition, macrophage infiltrations, and increasing the number of oxidative myofibers.[23]

This study aimed to evaluate the feasibility of a combination of pharmacological and nutraceutical approach based on MEK inhibitor and Cyanidin, respectively, as a treatment for MDs.

RESULTS

Trametinib decreases Nfix in postnatal myoblasts but not in fibroblasts and macrophages *in vitro*

To test the ability of Trametinib to decrease Nfix in postnatal myogenic cells as observed with PD98059,[13] we treated juvenile MuSC-derived myoblasts isolated from P10 WT mice with different concentrations of Trametinib with the aim of selecting the proper dosage of MEK inhibitor able to reduce both pERK and Nfix protein levels (Figure 1A). As expected, Trametinib-treated cells displayed a concentration-dependent inhibition of the ERK phosphorylation; moreover, 100 nM of Trametinib caused a consequent decrease in the Nfix protein levels of about 40% than the vehicle-treated cells (Figures 1B and 1C). Higher concentrations than 100 nM of Trametinib resulted in cell toxicity (data not shown), leading to apparent increase of the Nfix protein.

To understand whether this ERK-dependent modulation of Nfix occurs at post-transcriptional or post-translational rather than exclusively at transcriptional level as observed with PD98059,[13] we quantified the *Nfix* mRNA from 100 nM Trametinib and DMSO-treated myoblasts. As displayed in Figure 1D, the *Nfix* specific transcript did not change after treatment with Trametinib, revealing that the inhibition of MEK by the drug in juvenile myoblasts might affect Nfix at post translational rather than at transcriptional level.

Since lack of Nfix delays the myogenic differentiation *in vitro*,[10,13] we treated juvenile MuSC-derived myoblasts with DMSO or 100 nM of Trametinib and then we let them differentiate into myotubes for 4 days (Figure S1A). Although differentiation and fusion indexes did not change (data not shown), myotube length and maturation were evidently compromised by Trametinib, possibly due to Nfix reduction (Figure S1B).

Juvenile MuSC-derived myoblasts used for these experiments were not completely pure, and few Nfix-expressing fibroblasts could be still present in dishes. Therefore, we isolated and treated primary fibroblasts from murine muscles with different concentrations of Trametinib to exclude potential interference in the results. Indeed, fibroblasts treated *in vitro* with Trametinib presented concentration-dependent decreasing levels of pERK and increasing levels of Nfix protein compared to the control (Figures S1C and S1D), suggesting that the MEK/ERK pathway differently modulates Nfix protein abundance in fibroblasts and myoblasts.

Moreover, since we demonstrated the beneficial role of *Nfix*-lacking macrophages in dystrophic muscles,[12] we evaluated whether the MEK/ERK signaling cascade might regulate Nfix also in macrophages. Specifically, *in vitro*-polarized anti-inflammatory (M2) macrophages, which express higher level of Nfix than pro-inflammatory (M1) macrophages,[24] were treated with similar dosages of Trametinib used for juvenile MuSC-derived myoblasts. Despite an important inhibition of the ERK phosphorylation, M2 macrophages did not show a reduction of the Nfix protein after the treatment with Trametinib (Figures S1E and S1F).

These data revealed that the MEK/ERK pathway positively regulates Nfix in juvenile MuSC-derived myoblasts. This regulation is cell-type specific and occurs at post-transcriptional or -translational levels. Inhibiting the MEK/ERK pathway through Trametinib causes a reduction of the Nfix protein in myogenic cells *in vitro*.

Trametinib and Cyanidin treatment decreases the Nfix protein in *Sgca* null muscle

In accordance with specific treatment protocols described in literature for preclinical animal models of cancer, we decided to administer 3 mg/kg of Trametinib to adult *Sgca* null mice every day for 14 days by oral gavage, with the last dose received at least 4 h before sacrifice (Figure S2A). In this way, the drug maintains a systemic short-circulating half-life, potentially avoiding its side effects.[19,25–28] In addition, we combined the administration of Trametinib or its vehicle (DMSO) with the anthocyanin dietary regimen according to our previous study,[23] providing the Cyanidin as liquid diet at weaning for 5 weeks (Figure S2A).

Cyanidin was regularly consumed both before and during the administration of Trametinib. Indeed, there were no significant differences in consumed volume and animal weight between treated (Cyanidin+Trametinib) and control (Cyanidin+DMSO) groups of mice (Figures S2B

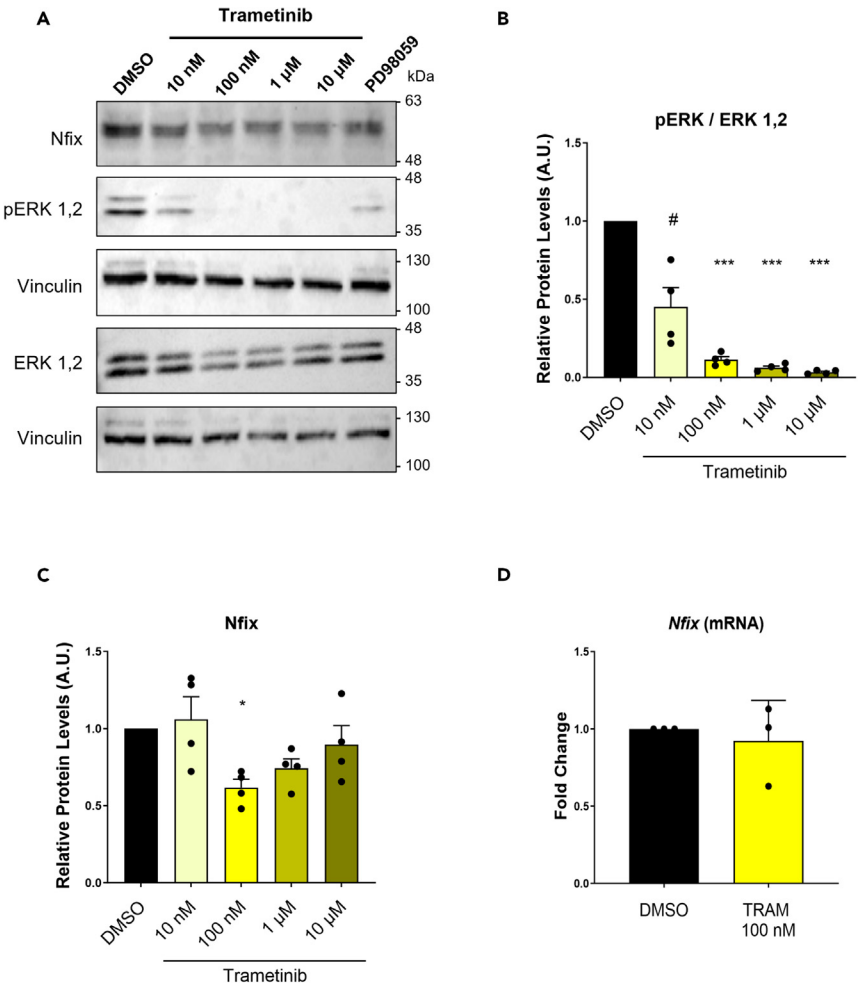

Figure 1. Trametinib decreases Nfix in postnatal myoblasts but not in fibroblasts and macrophages *in vitro*

(A) Representative western blots of juvenile MuSC-derived myoblasts treated with DMSO and different concentration of Trametinib *in vitro*, revealing protein levels of Nfix, ERK (pERK 1,2; ERK 1,2), and Vinculin used as house-keeping protein. PD98059-treated myoblasts were used as positive control.

(B and C) Quantitative densitometry from western blots of pERK/ERK 1,2 (B) and Nfix (C) protein levels in juvenile myoblasts treated with DMSO or Trametinib at different concentrations (data are presented as mean ± SEM; paired one-way ANOVA test, *: $p < 0.05$, ***: $p < 0.001$, #: $p = 0.0538$; n = 4).

(D) qRT-PCR evaluating the *Nfix* expression in juvenile MuSC-derived myoblasts treated with vehicle (DMSO) or 100 nM of Trametinib for 14 h. *β-actin* was used as house-keeping gene (data are presented as mean ± SEM; paired, two-tailed t-test, n = 3).

See also Figure S1.

and S2C). Moreover, Trametinib-treated mice did not present any visible phenotypical alterations than control, suggesting that Cyanidin was well-tolerated by mice and the combination with Trametinib did not cause any evident adverse effects to the general animal health.

To assess the inhibitory activity of Trametinib with or without Cyanidin, we analyzed the total protein lysate of dystrophic tibialis anterior muscles isolated from treated and control mice (Figure 2A). We have observed that 3 mg/kg of Trametinib caused a statistically significant reduction of pERK/ERK ratio (more than 70%) than the vehicle (Figure 2B), demonstrating that Trametinib properly inhibited the MEK/ERK pathway *in vivo*. In addition, Trametinib-treated muscles displayed a decreasing trend of the Nfix protein, although not statistically significant. Similarly, chronic administration of Cyanidin+Trametinib caused a significant reduction in pERK/ERK ratio and a similar decreasing trend in the Nfix protein to the control (Figures 2A and 2B).

The reduction of Nfix upon Trametinib and Cyanidin+Trametinib administration in dystrophic muscles was significant by immunofluorescence (IF) on dystrophic tibialis anterior (Figures 2C and 2D). Indeed, there is less Nfix-expressing ($Nfix^+$) nuclei in dystrophic muscles upon treatment with 3 mg/kg of Trametinib and Cyanidin+Trametinib than the controls. Specifically, Cyanidin+Trametinib treatment promoted a reduction of total $Nfix^+$ nuclei accounting for about 20% than the Cyanidin+DMSO control, at the same extent of what observed in Trametinib-treated muscles compared to DMSO group. Additionally, Cyanidin *per se* did not affect the number of the whole $Nfix^+$ nuclei compared to the DMSO controls (Figure 2D).

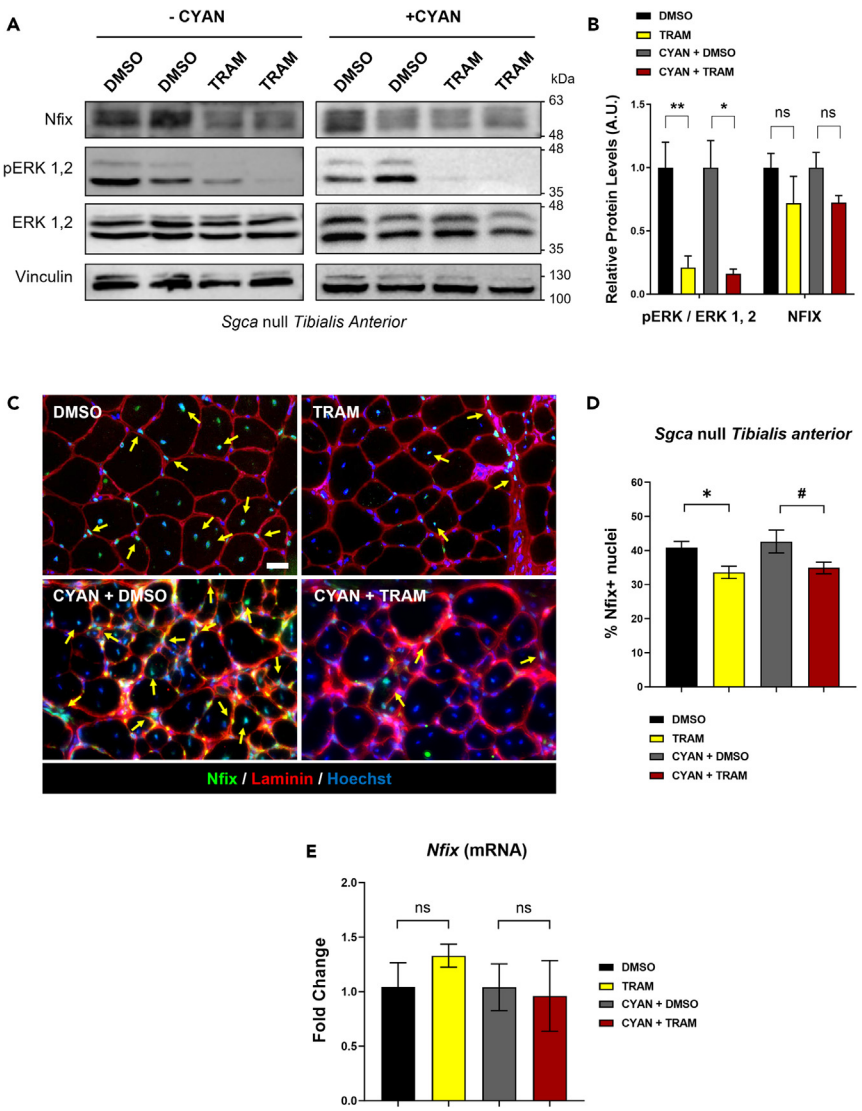

Figure 2. Trametinib and Cyanidin treatment decreases the Nfix protein in *Sgca* null muscle

(A) Representative western blots of total protein lysates from dystrophic tibialis anterior muscles treated with DMSO or Trametinib (TRAM), with (+CYAN) or without Cyanidin (-CYAN). Signals from Nfix, ERK (pERK 1,2; ERK 1,2), and Vinculin as house-keeping protein are depicted.

(B) Quantification by densitometric analysis of pERK/ERK 1,2 and Nfix protein levels in DMSO, TRAM, CYAN+DMSO, and CYAN+TRAM group of treated mice (data are presented as mean ± SEM; each data was normalized on the average value of its relative control; unpaired t-test, *: $p < 0.05$, **: $p < 0.01$; n = 5 for DMSO and TRAM, n = 3 for CYAN+DMSO, n = 4 for CYAN+TRAM).

(C) IF staining for Nfix (green), Laminin (red) and nuclei (Hoechst, blue) of tibialis anterior muscles from *Sgca* null mice treated with DMSO or Trametinib (TRAM), or in combination with Cyanidin (CYAN+DMSO; CYAN+TRAM). Yellow arrows indicate $Nfix^+$ nuclei; white bar = 50 μm.

(D) Graph depicting percentage of Nfix+ nuclei calculated from the IF in C (data are presented as mean ± SEM; unpaired t-test, *: $p < 0.05$, #: $p = 0.0601$; n = 5 for DMSO and TRAM; n = 3 for CYAN+DMSO; n = 4 for CYAN+TRAM).

(E) qRT-PCR evaluating the *Nfix* expression in tibialis anterior muscles from DMSO, TRAM, CYAN+DMSO, and CYAN+TRAM group of *Sgca* null mice. *β-actin* was used as house-keeping gene (data are presented as mean ± SEM; unpaired t-test; n = 5 for DMSO and TRAM, n = 3 for CYAN+DMSO, n = 4 for CYAN+TRAM). See also Figure S2.

The difference in the Nfix levels between the result from WB and the one from the IF was probably related to the different regulation of Nfix by the MEK/ERK pathway in both fibroblasts and macrophages than what occurs in myoblasts (Figures 1A–1C and S1C–S1F). Therefore, we decided to confirm this hypothesis by quantifying the $Nfix^+$ satellite cells *in vivo* avoiding interferences by Nfix-expressing fibroblasts or macrophages. We performed a muscle specific IF anti-Nfix and anti-Pax7 (paired box protein 7, a marker of satellite cells[29,30]) on control and treated tibialis anterior muscles. As indicated by our quantification (Figures S2D and S2E), both treatments with Trametinib and Cyanidin+Trametinib caused a statistically significant reduction of about 20% and 30% of $Pax7^+/Nfix^+$ cells, respectively, compared to the relative controls. This

reduction was higher than the one observed by quantifying the whole Nfix$^+$ cells (Figures 2C and 2D) or by Western Blot (Figure 2A). Moreover, the combination of Cyanidin+Trametinib caused a significant reduction of Nfix-expressing satellite cells compared to Trametinib alone, suggesting a synergistic effect of both treatments in reducing Nfix in satellite cells *in vivo*.

In line with what observed in myoblasts *in vitro*, qRT-PCR revealed that the *Nfix* gene expression did not change between muscles treated with Trametinib or Cyanidin+Trametinib and their relative controls (Figure 2E), supporting our previous data about a post-translational modulation of the Nfix protein abundance by the MEK/ERK pathway, also in presence of the Cyanidin diet.

Cyanidin administration reduces necrosis and fibrosis in Trametinib-treated dystrophic muscles

To evaluate whether Trametinib, Cyanidin or the combination of both compounds would lead to improvements of dystrophic phenotype, we analyzed the histology of treated and control muscles, comparing the main histological hallmarks of Cyanidin+Trametinib and Trametinib groups with the Cyanidin+DMSO and DMSO groups.

Firstly, we investigated the overall muscular architecture by Hematoxylin and Eosin (H&E) staining (Figure 3A). Unexpectedly, tibialis anterior and diaphragm muscles chronically treated with Trametinib exhibited more damaged areas than control muscles (DMSO). As demonstrated in our previous work, Cyanidin reduces the oxidative stress, alleviating dystrophic muscles from damages and fibrotic tissue.[23] Indeed, Cyanidin-treated muscles exhibited fewer fibrotic and scar tissue than the Trametinib and DMSO groups (Figure 3A). Nevertheless, similarly to the DMSO counterpart, Cyanidin-treated muscles reported a non-homogeneous cross-sectional area (CSA) of myofibers, clearly indicating a dystrophic phenotype (Figures S3A and S3B).

Concerning muscle regeneration, we evaluated the percentage of centrally nucleated myofibers among our treated animals. Trametinib administration did not significantly alter the number of centrally nucleated myofibers compared to DMSO-treated muscles (Figures S3C and S3D). On the other side, Cyanidin treatment decreased the number of centrally nucleated fibers compared to DMSO and Trametinib-treated animals regardless Trametinib co-administration as shown in (Figures S3C and S3D), indicating that this parameter is mainly related to Cyanidin *per se* rather than to the combination with MEK-inhibition.

Since necrosis and fibrosis are the main hallmarks of the dystrophic muscle, we assessed them by IF for immunoglobulin G (IgG) and Collagen-I, respectively[31,32] (Figure 3B). Tibialis anterior muscles treated with Trametinib displayed a significant increase in the amount of degenerating myofibers compared to DMSO control. Interestingly, this condition was completely rescued by the addition of Cyanidin to Trametinib treatment: indeed, Cyanidin+Trametinib-treated muscles exhibited a comparable amount of necrosis to the Cyanidin+DMSO group. Contrarily, the Trametinib-induced increase of IgG$^+$ myofibers was not rescued by Cyanidin+Trametinib in dystrophic Diaphragms (Figure 3C).

As regards fibrosis, while Trametinib did not cause any difference in fibrotic deposits in tibialis anterior muscles compared to the DMSO control, Cyanidin+Trametinib treatment promoted a reduction in Collagen-I deposits, accounted for about 9% than the Trametinib group. Similarly, Cyanidin+DMSO resulted in a remarkable decrease in fibrosis of about 15%, compared to the DMSO counterpart (Figures 3D and 3E). As observed for necrosis, Cyanidin has no effect on Collagen I deposits in Diaphragm, while Trametinib promoted fibrotic deposition (Figure 3E).

These data suggest a muscle-dependent positive effect of Cyanidin in rescuing the impact of Trametinib on necrosis and fibrosis in dystrophic muscles.

Trametinib decreases adipose tissue deposits in dystrophic muscles

The fatty acid deposits are another important hallmark of impaired muscle regeneration and muscular dystrophy. To evaluate this histological parameter, we performed the Oil Red-O staining on treated and control muscles (Figure 4A). Fatty acid deposits were vividly red stained in both DMSO and Cyanidin+DMSO muscles, particularly in Diaphragm where adipose tissues occupied a wider area between myofibers compared to what observed in tibialis anterior. Interestingly, treatment with Trametinib seemed to reduce the extension of adipose tissue, regardless of Cyanidin supplementation.

To understand if the decrease in fatty-acid deposits was related to changing in the number of fibro-adipogenic progenitors cells (FAPs), we quantified the number of PDGFRα^+ cells (Platelet-derived Growth Factor Receptor alpha) as pan-marker of FAPs[33] (Figure 4B). We observed a general slight increase of PDGFRα^+ cell number after the administration of Cyanidin in both tibialis anterior and diaphragm (DMSO vs. CYAN+DMSO, and TRAM vs. CYAN+TRAM). However, chronic treatment with Trametinib did not reduce the number of FAPs in Cyanidin treated mice (Figure 4C), suggesting that MEK-inhibition might affect the differentiation into adipocytes rather than the proliferation of FAPs.

Chronic MEK-inhibition causes ectopic calcifications in dystrophic but not in WT muscles

As visible in H&E staining of Trametinib-treated muscles (Figure 3A), chronic administration of Trametinib unexpectedly caused visible histological alterations in dystrophic tibialis anterior and in diaphragm. These alterations appeared as thick, dark myofibers at H&E staining and they overlapped with areas of high degeneration and immune infiltration. Since Duclos et al. described similar histological signs in *Sgca* null muscles as uncommon dystrophic calcifications,[20] we used Alizarin Red to specifically stain muscular calcifications (MCs) in DMSO and Trametinib-treated muscles (Figure 5).

Although faint Alizarin Red-positive myofibers were rarely detected in DMSO-treated *Sgca* null muscles, MCs were stained in vivid red in both tibialis anterior and diaphragm after the treatment with Trametinib (Figures 5A, 5B, and S4A). Frequently MCs emerged clustered, especially in areas greatly affected by dystrophic degeneration. Upon quantification, we revealed a significant increase in the areas occupied by

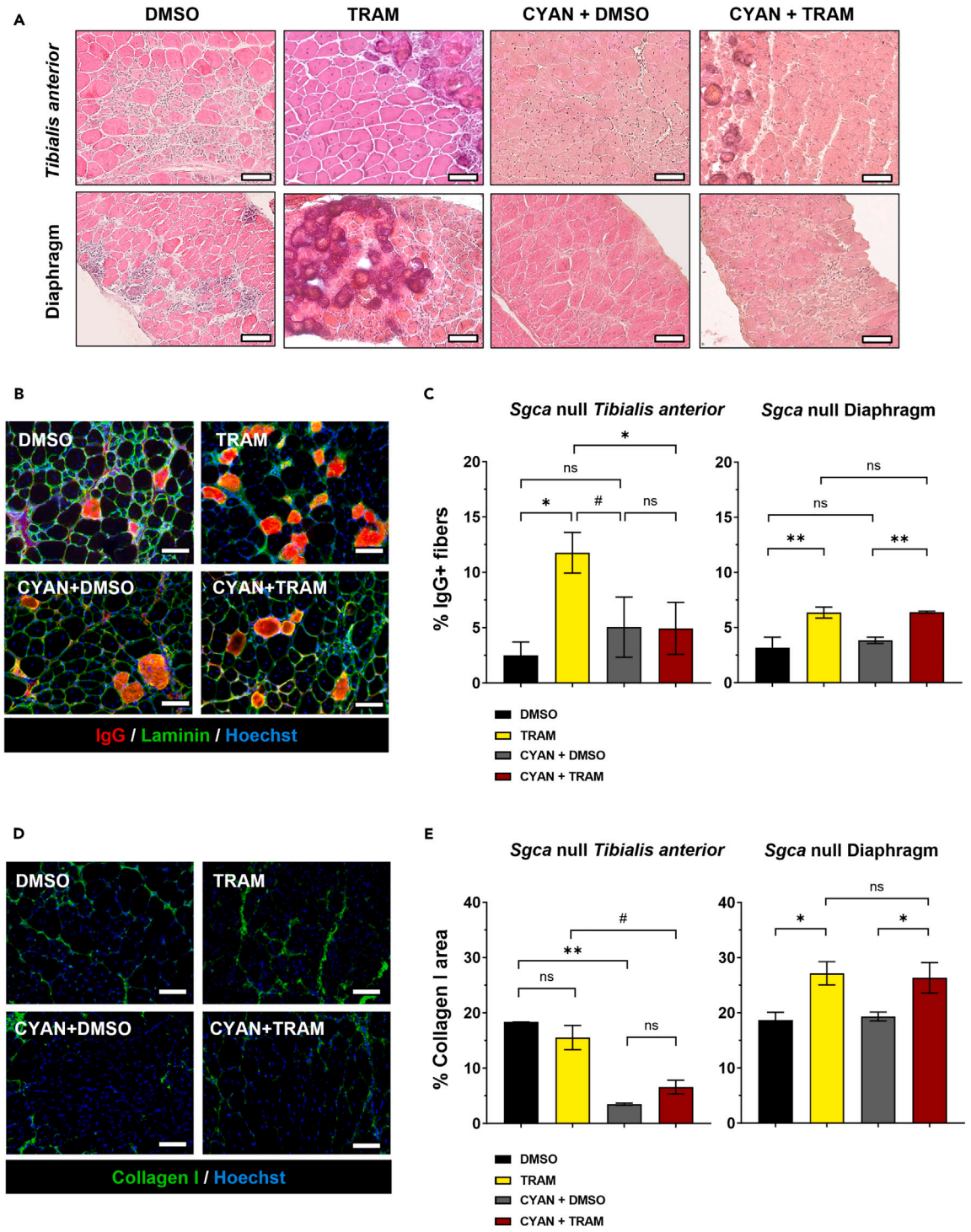

Figure 3. Cyanidin reduces necrosis and fibrosis in Trametinib-treated dystrophic muscles

(A) Hematoxylin and eosin of tibialis anterior and diaphragm muscles from DMSO, TRAM, CYAN+DMSO, and CYAN+TRAM group of *Sgca* null mice. White bar = 100 μm.

(B and D) Immunofluorescence staining of tibialis anterior muscles from DMSO, TRAM, CYAN+DMSO, and CYAN+TRAM group of *Sgca* null mice identifying (B) IgG+ fibers in red, Laminin in green, total nuclei with Hoechst in blue, and (D) Collagen-I in green and total nuclei in blue. White bar = 100 μm.

(C and E) Graphs depicting relative quantifications of (C) IgG+ fibers and (E) Collagen-I deposits from dystrophic muscles (data are presented as mean ± SEM; one-way ANOVA, **: $p < 0.01$, #: $p = 0.097$; n = 5 for DMSO and TRAM, n = 3 for CYAN+DMSO, n = 4 for CYAN+TRAM).

See also Figure S3.

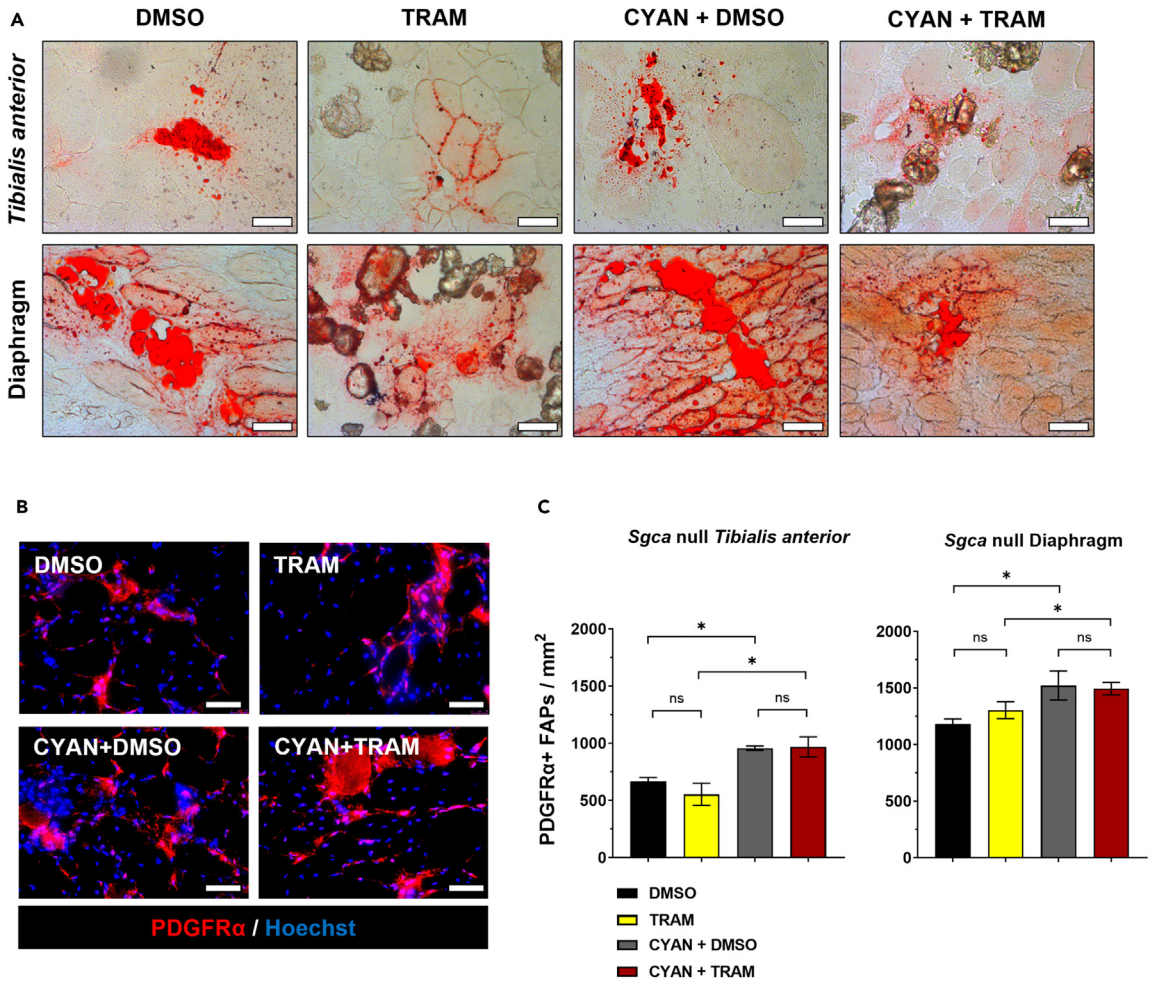

Figure 4. Trametinib decreases adipose tissue deposition in dystrophic muscles

(A) Oil Red-O staining on *Tibialis anterior* and Diaphragm muscles from DMSO, TRAM, CYAN+DMSO, and CYAN+TRAM group of *Sgca* null mice (white bar = 50 μm).

(B) IF on PDGFRα (in red) and nuclei (Hoechst, in blue) in tibialis anterior muscles from DMSO, TRAM, CYAN+DMSO, and CYAN+TRAM group of *Sgca* null mice.

(C) Relative quantification of PDGFRα+ FAPs in tibialis anterior and diaphragm muscles (data are presented as mean ± SEM; one-way ANOVA, *: $p < 0.05$, n = 5 for DMSO and TRAM; n = 3 for CYAN+DMSO; n = 4 for CYAN+TRAM; white bar = 50 μm).

MCs after the treatment of Trametinib, particularly in *Sgca* null Diaphragms, which reported a worse condition than Trametinib-treated tibialis anterior muscles with a calcified tissue area of about 14% (Figure 5B). We also observed that MCs were present in soleus and gastrocnemius (Figures S5C and S5D) muscles after the treatment with Trametinib.

To attest whether these unexpected MCs are related to either the treatment with MEK inhibitor and/or the *Sgca* null genetic background, we treated age-matched wildtype (WT) and *dystrophin*-deficient (*mdx*) mice[34] with the same protocol and dose of Trametinib used for *Sgca* null mice. Interestingly, Trametinib treatment caused the deposition of MCs also in *mdx* muscles at the same extent as what observed in *Sgca* null mice, covering an average area of about 6% in tibialis anterior and 11% in Diaphragm (Figures 5A and 5B). Conversely, WT muscles did not display MCs after the treatment with Trametinib (Figure 5A), suggesting that chronic MEK-inhibition induces calcifications only in a dystrophic milieu, regardless of the genetic background or mutation.

MCs could be a peculiar side effect specifically induced by Trametinib in a dystrophic context. To test this hypothesis, we fortnightly treated 6-week-old *Sgca* null mice with 25 mg/kg of Selumetinib, an MEK inhibitor used in preclinical studies as a potential treatment for cancer, cachexia, and in a phase II clinical trial against neurofibromatosis type 1 (NCT02407405).[35,36] Intriguingly, Selumetinib-treated muscles exhibited MCs in both tibialis anterior and diaphragm dystrophic muscles as observed with Trametinib (Figure S4B), markedly denoting that these histological alterations are induced by a chronic MEK-inhibition in a dystrophic muscle despite the type of drug used.

We next investigated whether the Trametinib-induced MCs were related to the muscular dystrophy *per se* or to the degeneration/regeneration process that constantly occurs in dystrophic muscles. To assess this aspect, we injured tibialis anterior of WT mice with Cardiotoxin

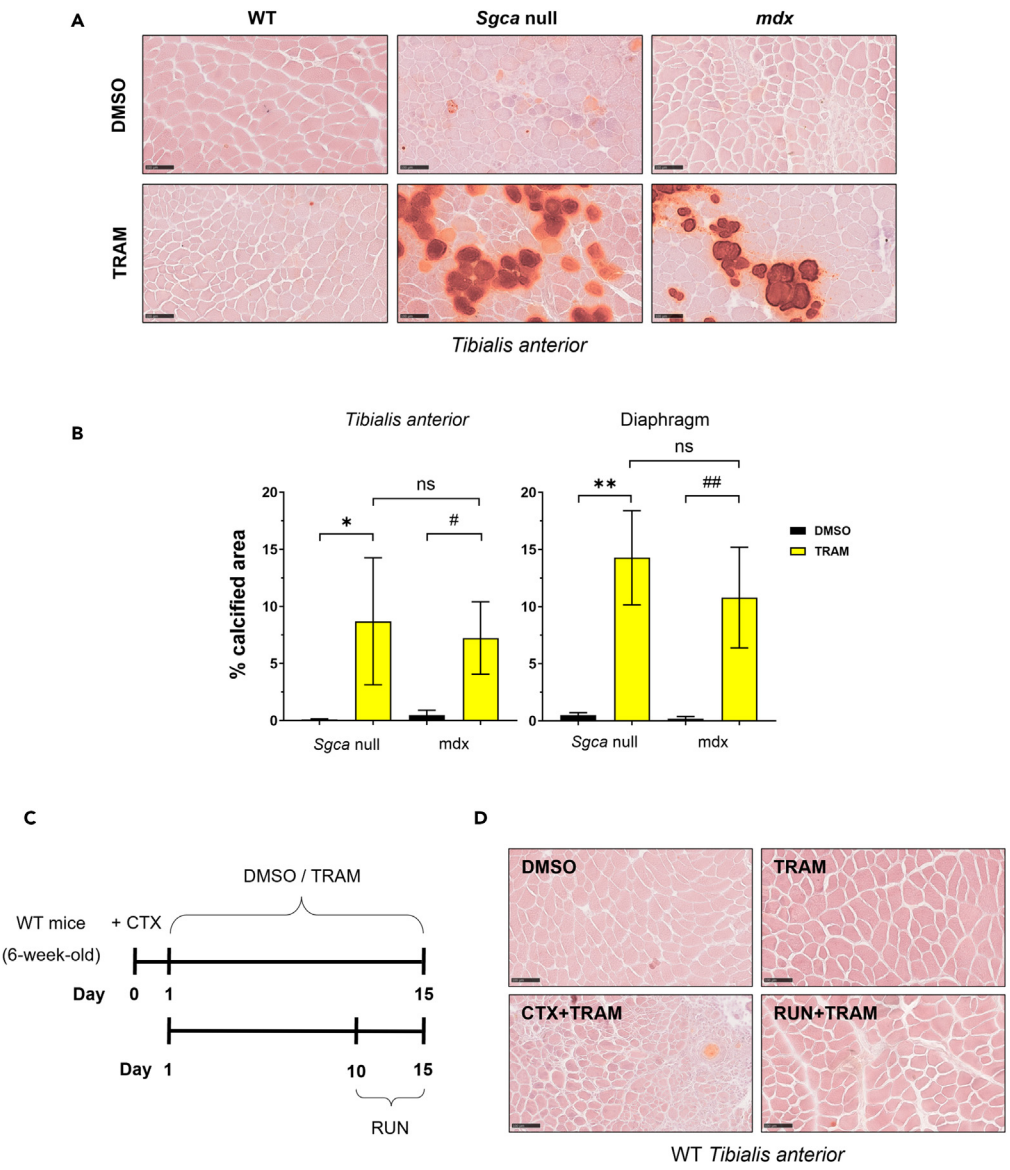

Figure 5. Chronic MEK-inhibition causes ectopic calcifications in dystrophic but not in WT muscles

(A) Alizarin Red staining of tibialis anterior muscles from WT, *Sgca* null and *mdx* mice chronically treated with DMSO or Trametinib (TRAM). Black bar = 100 μm.

(B) Graphs depicting the calcified area from Alizarin Red-stained tibialis anterior and diaphragm muscles isolated from mice described in A (data are presented as mean ± SEM; one-way ANOVA, *: $p < 0.05$, **: $p < 0.01$, #: $p = 0.0715$, ##: $p = 0.0910$; n = 3 for WT and *mdx*, n = 5 for DMSO and TRAM *Sgca* null).

(C) Scheme of treatment for CTX-induced injury (CTX) or strenuous exercise (RUN) of Trametinib-treated WT mice (6-week-old).

(D) Alizarin Red staining of tibialis anterior muscles from WT mice treated with DMSO, TRAM, CTX+TRAM, or RUN+TRAM (treatment with Trametinib + strenuous exercise). Contralateral, not-injured tibialis anterior was used as Trametinib-treated control (TRAM). Black bar = 100 μm. (n = 3 for DMSO, TRAM, CTX+TRAM, and RUN+TRAM, each).

See also Figure S4.

(CTX), inducing degeneration and consequent regeneration into the muscle, and we chronically administered Trametinib 1-day after CTX injection by oral gavage for 14 days (Figure 5C). Surprisingly, CTX-injured muscles from WT mice did not display any signs of MCs upon Trametinib administration, besides a faint Alizarin Red staining overlapped with the injection site (Figure 5D).

Moreover, we investigated whether strenuous exercise could make WT muscles more susceptible to Trametinib-induced MCs. Therefore, we forced DMSO- and Trametinib-treated WT mice to a constant downhill exercise for 30 min per day for 5 days. Since treatment with Trametinib lasted 14 days, we tested the effect of the strenuous exercise on treated muscles at the end of the pharmacological treatment, overlapping the two protocols (Figure 5C). Tibialis anterior muscles from exercised WT mice displayed signs of strenuous training and damage, such as more developed blood-vessels and fibrosis, compared to sedentary muscle. However, in Trametinib-treated WT muscles we did not

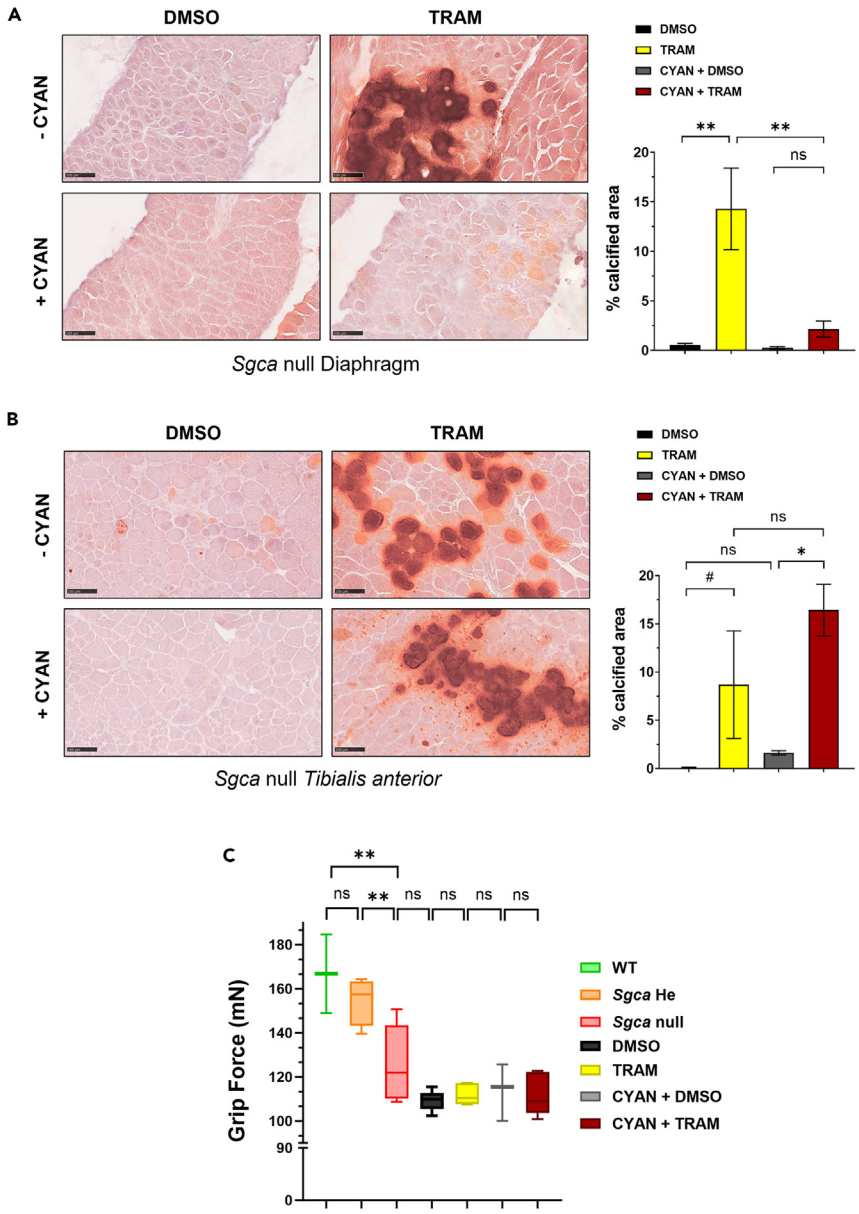

Figure 6. Cyanidin prevents Trametinib-induced ectopic calcifications in dystrophic Diaphragm and Soleus

(A and B) Alizarin Red staining of diaphragm (A) and tibialis anterior (B) muscles with graphs showing relative calcified area (on the right) from DMSO, TRAM, CYAN+DMSO, and CYAN+TRAM group of *Sgca* null mice (data are presented as mean ± SEM; one-way ANOVA, *: $p < 0.05$, **: $p < 0.01$; n = 5 for DMSO and TRAM; n = 3 for CYAN+DMSO; n = 4 for CYAN+TRAM; black bar = 100 μm).

(C) Total muscular force (expressed in mN) from wildtype (WT), *Sgca* heterozygous (*Sgca* He), *Sgca* null, CYAN+DMSO *Sgca* null, and CYAN+TRAM *Sgca* null mice (data are presented as mean and min to max; one-way ANOVA, **: $p < 0.01$; n = 3 for WT, n = 4 for *Sgca* He, n = 5 for *Sgca* null, n = 3 for CYAN+DMSO, n = 4 for CYAN+TRAM).

See also Figure S5.

observe any MCs by the Alizarin Red staining (Figure 5D), suggesting that these histological alterations are peculiar to MEK-inhibited dystrophic muscles.

Cyanidin prevents Trametinib-induced ectopic calcifications in dystrophic Diaphragm and Soleus

We then evaluated the extent of MCs in dystrophic muscles treated with Cyanidin+Trametinib. As expected, DMSO and Cyanidin+DMSO-treated muscles did not exhibit calcifications (Figures 6A and 6B). Surprisingly, Cyanidin+Trametinib treatment promoted a statistically significant reduction of Trametinib-induced MCs in Diaphragms, covering an average area of 2% rather than the 14% (Figure 6A). Conversely,

dystrophic tibialis anterior muscles exhibited an increasing trend in MCs' area in Cyanidin+Trametinib than Cyanidin+DMSO control, at the same extent of Trametinib-treated counterparts without Cyanidin supplementation (Figure 6B). The same positive effect of Cyanidin in decreasing Trametinib-induced MCs was also detectable in *Soleus* (FigureS5C) but not in *Gastrocnemius* muscles (FigureS5D).

Since in the *mdx*$^{\beta geo}$ mouse model similar calcium deposits were described as spontaneous histological alterations strongly associated with macrophage infiltrations,[37] we quantified the F4/80^{+} macrophages' area in control and treated muscles (Figures S5A and S5B). Interestingly, macrophage infiltrations showed similar trend to MCs: both Trametinib-treated tibialis anterior and diaphragm displayed an increase of infiltrating macrophages, which was rescued by the supplementation of Cyanidin in Diaphragm but not in tibialis anterior (Figure S5B). Collectively, these results demonstrate that Cyanidin rescued or prevented calcifications caused by Trametinib in some muscles, such as Diaphragm and *Soleus*.

Furthermore, we analyzed the possibility of reabsorption of MCs stopping the administration of Trametinib in combination or not with Cyanidin. Indeed, 2 weeks post last dose of Trametinib, tibialis anterior muscles displayed less MCs compared to relative fortnightly treated muscles, independently to Cyanidin supplementation (Figure S5E).

Finally, to evaluate whether the MCs could affect the functionality of hindlimb muscles, muscle force was measured by grip test. Specifically, the grip test allows the measurement of maximal muscle strength from a combination of forelimb and hindlimb muscles. As expected, 8-week-old heterozygotic *Sgca* (*Sgca* He) and dystrophic *Sgca* null mice exhibited lower force compared to age-matched WT mice, indicating that the test is highly reliable. We observed no difference in grip strength between Cyanidin treated animals with or without Trametinib (Figure 6C). Hence, the combination of Cyanidin and Trametinib did not influence the total muscle force and the presence of MCs did not affect the overall functionality of hindlimb muscles.

DISCUSSION

MDs are a group of myopathies which are extremely heterogeneous basing on age of onset, severity, and prognosis. A limiting factor for all the latest therapies is the degree of degeneration of the dystrophic muscles, which strongly impairs patients' eligibility to the most promising gene and cell therapies. Therefore, it is necessary to promote combined approaches consisting of both curative treatment (targeting the causative mutations) and conservative treatment, which aims to ameliorate muscle histology and increase the therapeutic efficacy of the first.[38]

Nfix regulates many processes in post-natal muscle, ranging from the timing of muscle regeneration, macrophage skewing, and fiber type determination.[8,10,24] Notably, we demonstrated that silencing Nfix in dystrophic mice preserves dystrophic muscles from the degeneration,[11] electing Nfix as a potential therapeutic target in MDs. Our efforts in these years were focused on defining the regulatory network underlying Nfix at transcriptional, post-transcriptional, and post-translational levels in muscle cells. Our results on MEK/ERK-dependent regulation of Nfix during embryo-fetal myogenesis, both *in vitro* and *in vivo*,[13] prompted us to develop a pharmacological approach to inhibit Nfix also in adult dystrophic mice with the aim of improving muscle histology and functionality.

In this study, we have provided the proof-of-concept that a chronic treatment with the FDA-approved MEK inhibitor Trametinib decreases Nfix in adult dystrophic muscles. This modulation occurs at the protein levels in satellite cells, confirming what we previously observed after the treatment of myoblasts *in vitro* with another MEK inhibitor.[13] However, the resulting reduction of the Nfix protein upon the treatment with Trametinib is not sufficient to improve the pathology. Since we recently demonstrated the role of Nfix$^{-/-}$ macrophages in improving the dystrophic phenotype,[12] the lack of Trametinib effect on Nfix in these cells strongly attenuates the histologic ameliorations by the drug. Furthermore, the combination of Trametinib and Cyanidin promotes the same histological rescue observed in the co-treatment versus the Trametinib alone, suggesting that the antioxidant *per se* mainly prevents the downsides of the drug.

Additionally, we observed that chronic MEK-inhibition unexpectedly causes calcifications specifically in dystrophic skeletal muscles, representing a limitation of this treatment. None of pre-clinical and clinical studies on Trametinib-treated animal models and oncologic patients described this peculiar effect on muscle histology, so far.[39–41] In literature, MCs are considered as the starting stage of Heterotopic Ossifications (HO) in soft tissues,[42,43] which characterize some severe genetic diseases like fibrodysplasia ossificans progressiva (FOP).[44] In WT skeletal muscles, MCs are only induced by severe injury, like blast trauma,[45] or by Notexin injection.[46] Although uncommon in *mdx* and *Sgca* null mice, MCs spontaneously occur in other dystrophic mouse models (particularly in Diaphragm) with different types of genetic mutations, like in the *mdx*$^{\beta geo}$,[37] the D2-*mdx*,[47] and the immunodeficient *Sgcb*-null mice.[48] These dystrophic models are characterized by higher degree of necrosis, fibrosis and inflammation, and MCs represent a sign of worsened pathologic conditions. In our study, we highlighted for the first time that MCs occur in dystrophic but not in regenerating or exercised WT muscle upon chronic MEK-inhibition, independently of the MEK inhibitor used, the genetic background underlying MDs, or eventual impairments in the degeneration/regeneration process due to MAPK pathway inhibition. Moreover, MCs are not related to the decrease of Nfix, as suggested by *Sgca* null/*Nfix* null mice which do not display these histological alterations.[11]

As observed in *mdx*$^{\beta geo}$ and D2-*mdx* mice, these MEK inhibitor-related MCs are present in different dystrophic muscles, both hindlimb and respiratory muscles, and are partly re-absorbed in tibialis anterior after 2 weeks since the last dose of Trametinib. Moreover, testing the combination of Cyanidin and Trametinib in improving dystrophic pathology, we observed a muscle-specific positive effect of Cyanidin in rescuing Trametinib-induced MCs. Indeed, 5-week Cyanidin-diet regimen preserves Diaphragms and Soleus but not tibialis anterior and *gastrocnemius* from developing MCs in *Sgca* null mice. Crossing all the results from histological analyses, we can conclude that this muscle-specific amelioration by Cyanidin is unrelated to necrosis and fibrosis. Indeed, the Cyanidin+Trametinib combination preserves Trametinib-treated tibialis anterior from the increase of necrosis and fibrosis but not from calcifications; the opposite is for Diaphragm, which

Cyanidin relieves from MCs but not from necrosis and Collagen-I deposition. Hence, we can assume that MCs do not derive from necrotic myofibers or Collagen-I deposits, and that MEK-inhibition is the triggering signal for the deposition of MCs in a dystrophic context.

Concerning the origin of these calcium deposits, all the scientific studies on HO agree about the crucial role of FAPs in generating them in muscle tissue.[33] Besides the differentiation into fibroblasts and adipocytes, FAPs can acquire osteogenic phenotype both *in vitro*[49,50] and *in vivo*,[43,51] and different stimuli lead them to produce calcification in skeletal muscles. To sum up, the asynchronous inflammation of the dystrophic milieu, with high levels of TGF-β (especially in D2-*mdx* muscle),[50] and/or BMP2[51,52] can reprogram resident FAPs toward the osteogenic behavior. Several papers suggest that the MAPK pathway promotes adipocyte differentiation of FAPs,[53,54] while the genetic deletion of both ERK1/2 in osteocytes stimulates calcium deposition.[55] Interestingly, plasminogen-deficient *mdx* mice display high degree of MCs[56] and the MEK-inhibition leads to the upregulation of the plasminogen activator inhibitor-1 (PAI-1).[57] Our results reported here confirm that Trametinib strongly reduces the accumulation of adipose tissue in dystrophic muscles without affecting the density of muscle resident FAPs. Understanding whether MEK inhibitor and the dystrophic milieu directly or indirectly impinge the FAPs' cell-fate, blocking their adipogenic differentiation and pushing them toward transitory osteogenic behavior, might provide useful insights for basic and clinical research on HO or FOP.[44,58–60]

We also demonstrated that another MEK inhibitor, Selumetinib, triggers MCs in dystrophic muscles. Intriguingly, Selumetinib was tested in a murine model of Emery-Dreifuss Muscular Dystrophy (EDMD), but the authors did not notice calcifications in treated muscles.[61] Although classified as MD, EDMD has distinct pathological features than Duchenne muscular dystrophy (DMD) or sarcoglycanopathies, like the genetic mutation, the degree of inflammation, and other pathological hallmarks.[62] This different susceptibility to MCs induced by MEK-inhibition between EDMD and DMD muscles might reveal novel subtypes of FAPs in various MDs, underrated so far.

Related to this, the specific rescue of MCs in diaphragm and not in tibialis anterior by Cyanidin might give some interesting insights. A very recent paper demonstrated the presence by single cell RNA-seq of different populations of FAPs between *mdx* diaphragm and quadriceps. Specifically, FAPs in *mdx* Diaphragm acquire a unique stressed phenotype, which is more prone in responding to the inflammatory microenvironment and is absent in *mdx* Quadriceps.[63] Deeper studies to assess whether Cyanidin might directly interfere with stressed FAPs' metabolism in the dystrophic milieu are required.

Finally, these serendipitous results on MCs after treatment with MEK inhibitor and/or Cyanidin will provide different cues about other scientific questions. For instance, the recent work by Boyer et al. undoubtedly demonstrated that the genetic deletion of ERK in $Pax7^{+}$ MuSC leads to a depletion of satellite cells and consequent histological improvements in adult dystrophic muscles.[64] This apparently counterintuitive statement reveals the importance of delaying rather than boosting muscle regeneration in dystrophic muscles to better achieve a more efficient therapeutic outcome. However, a novel pharmacological approach targeting the MEK/ERK pathway of MuSCs in dystrophic muscle might cause various and unexpected side effects, as our study proved.

Limitations of the study

In this study, we highlighted the correlation between MEK-inhibition and the decrease of Nfix in myogenic cells of murine dystrophic muscles. This modulation occurs at the protein levels, but the underlying molecular mechanism as well as the reason behind the cell-specific effect of Trametinib on Nfix remains unclear. Moreover, which cell type Trametinib-induced calcifications originate from and why the antioxidant effect of Cyanidin partially rescues them are still open questions.

Follow-up studies are ongoing to collect more information about post-translational modifications of Nfix and the possible involvement of FAPs upon treatment with Trametinib in dystrophic muscles. The development of these issues will be relevant for those clinical trials based on MEK inhibitors and the pathophysiology of muscular dystrophy.

STAR★METHODS

Detailed methods are provided in the online version of this paper and include the following:

- KEY RESOURCES TABLE
- RESOURCE AVAILABILITY
  - Lead contact
  - Materials availability
  - Data and code availability
- EXPERIMENTAL MODEL AND STUDY PARTICIPANT DETAILS
  - Wildtype C57BL/6J, Sgca null, and mdx mice
  - Wildtype CD1 mice, primary myoblasts and fibroblasts
  - Primary macrophage cell culture
- METHOD DETAILS
  - Drug treatment *in vitro*
  - Treatment with MEK-inhibitors *in vivo*
  - Cyanidin-enriched diet
  - Grip strength test
  - Forced downhill strenuous exercise

- Protein extraction and western blotting
- RNA extraction and qRT-PCR
- Inclusion and cryo-sectioning of muscles
- Immunofluorescence
- Hematoxylin & eosin staining
- Alizarin Red staining
- Oil Red O staining
- Cross-sectional area and myotube length

- QUANTIFICATION AND STATISTICAL ANALYSIS

SUPPLEMENTAL INFORMATION

Supplemental information can be found online at https://doi.org/10.1016/j.isci.2023.108696.

ACKNOWLEDGMENTS

We thank R. Gronostajski for the kind exchange of information and animal models. We are also grateful to thank G. Caretti and L. Nevi for their help on grip test and kind lend of the dynamometer.

We thank NoLimits imaging facility at University of Milan for histological images.

This research was funded by the "Association Française contre les Myopathies, AFM-Téléthon" (Grant number 23156).

AUTHOR CONTRIBUTIONS

G.A., conceptualization, data curation, formal analysis, investigation, project administration, supervision, validation, visualization, writing – original draft, writing – review and editing.

E.C., F.R., V.T., and C.B. data curation, formal analysis, investigation, validation, visualization of data from *in vivo* samples, and writing – review and editing.

G.Mu., G.R., R.F., G.C., and M.S. data curation, formal analysis, investigation, validation, visualization of data from *in vitro* experiments, and writing – review and editing.

G.Me., conceptualization, funding acquisition, project administration, resources, supervision, validation, writing – original draft, writing – review and editing.

All authors read and approved the final paper.

DECLARATION OF INTERESTS

The authors declare no competing interests.

Received: March 1, 2023
Revised: October 3, 2023
Accepted: December 6, 2023
Published: December 10, 2023

REFERENCES

1. Mercuri, E., Bönnemann, C.G., and Muntoni, F. (2019). Muscular dystrophies. Lancet *394*, 2025–2038.
2. Shin, J., Tajrishi, M.M., Ogura, Y., and Kumar, A. (2013). Wasting mechanisms in muscular dystrophy. Int. J. Biochem. Cell Biol. *45*, 2266–2279.
3. Rahimov, F., and Kunkel, L.M. (2013). Cellular and molecular mechanisms underlying muscular dystrophy. J. Cell Biol. *201*, 499–510.
4. McDonald, C.M., Henricson, E.K., Abresch, R.T., Duong, T., Joyce, N.C., Hu, F., Clemens, P.R., Hoffman, E.P., Cnaan, A., Gordish-Dressman, H., et al. (2018). Long-term effects of glucocorticoids on function, quality of life, and survival in patients with Duchenne muscular dystrophy: a prospective cohort study. Lancet, 32160–32168.
5. Choi, E., and Koo, T. (2021). CRISPR technologies for the treatment of Duchenne muscular dystrophy. Mol. Ther. *29*, 3179–3191.
6. Galli, F., Bragg, L., Meggiolaro, L., Rossi, M., Caffarini, M., Naz, N., Santoleri, S., and Cossu, G. (2018). Gene and Cell Therapy for Muscular Dystrophies: Are We Getting There? Hum. Gene Ther. *29*, 1098–1105.
7. Chen, K.S., Lim, J.W.C., Richards, L.J., and Bunt, J. (2017). The convergent roles of the nuclear factor I transcription factors in development and cancer. Cancer Lett. *410*, 124–138.
8. Messina, G., Biressi, S., Monteverde, S., Magli, A., Cassano, M., Perani, L., Roncaglia, E., Tagliafico, E., Starnes, L., Campbell, C.E., et al. (2010). Nfix Regulates Fetal-Specific Transcription in Developing Skeletal Muscle. Cell *140*, 554–566.
9. Pistocchi, A., Gaudenzi, G., Foglia, E., Monteverde, S., Moreno-Fortuny, A., Pianca, A., Cossu, G., Cotelli, F., and Messina, G. (2013). Conserved and divergent functions of Nfix in skeletal muscle development during vertebrate evolution. Development *140*, 2443.
10. Rossi, G., Antonini, S., Bonfanti, C., Monteverde, S., Vezzali, C., Tajbakhsh, S., Cossu, G., and Messina, G. (2016). Nfix Regulates Temporal Progression of Muscle Regeneration through Modulation of Myostatin Expression. Cell Rep. *14*, 2238–2249.
11. Rossi, G., Bonfanti, C., Antonini, S., Bastoni, M., Monteverde, S., Innocenzi, A., Saclier, M., Taglietti, V., and Messina, G. (2017). Silencing Nfix rescues muscular dystrophy by delaying muscle regeneration. Nat. Commun. *8*, 1055–1112.
12. Saclier, M., Angelini, G., Bonfanti, C., Mura, G., Temponi, G., and Messina, G. (2022). Selective ablation of Nfix in macrophages attenuates muscular dystrophy by inhibiting fibro-adipogenic progenitor-dependent fibrosis. J. Pathol. *257*, 352–366.

13. Taglietti, V., Angelini, G., Mura, G., Bonfanti, C., Caruso, E., Monteverde, S., Le Carrou, G., Tajbakhsh, S., Relaix, F., and Messina, G. (2018). RhoA and ERK signalling regulate the expression of the transcription factor Nfix in myogenic cells. Development *145*, dev163956.
14. Montagut, C., and Settleman, J. (2009). Targeting the RAF-MEK-ERK pathway in cancer therapy. Cancer Lett. *283*, 125–134.
15. Yuan, J., Dong, X., Yap, J., and Hu, J. (2020). The MAPK and AMPK signalings: Interplay and implication in targeted cancer therapy. J. Hematol. Oncol. *13*, 113–119.
16. Rutkowski, P., Lugowska, I., Kosela-Paterczyk, H., and Kozak, K. (2015). Trametinib: a MEK inhibitor for management of metastatic melanoma. OncoTargets Ther. *2251*, 2251.
17. Campbell, C.E., Piper, M., Plachez, C., Yeh, Y.T., Baizer, J.S., Osinski, J.M., Litwack, E.D., Richards, L.J., and Gronostajski, R.M. (2008). The transcription factor Nfix is essential for normal brain development. BMC Dev. Biol. *8*, 52.
18. Heng, Y.H.E., McLeay, R.C., Harvey, T.J., Smith, A.G., Barry, G., Cato, K., Plachez, C., Little, E., Mason, S., Dixon, C., et al. (2014). NFIX regulates neural progenitor cell differentiation during hippocampal morphogenesis. Cerebr. Cortex *24*, 261–279.
19. Gilmartin, A.G., Bleam, M.R., Groy, A., Moss, K.G., Minthorn, E.A., Kulkarni, S.G., Rominger, C.M., Erskine, S., Fisher, K.E., Yang, J., et al. (2011). GSK1120212 (JTP-74057) is an inhibitor of MEK activity and activation with favorable pharmacokinetic properties for sustained in vivo pathway inhibition. Clin. Cancer Res. *17*, 989–1000.
20. Duclos, F., Straub, V., Moore, S.A., Venzke, D.P., Hrstka, R.F., Crosbie, R.H., Durbeej, M., Lebakken, C.S., Ettinger, A.J., van der Meulen, J., et al. (1998). Progressive muscular dystrophy in α-sarcoglycan-deficient mice. J. Cell Biol. *142*, 1461–1471.
21. Pasteuning-Vuhman, S., Putker, K., Tanganyika-De Winter, C.L., Boertje-Van Der Meulen, J.W., van Vliet, L., Overzier, M., Plomp, J.J., Aartsma-Rus, A., and van Putten, M. (2017). Natural disease history of mouse models for limb girdle muscular dystrophy types 2D and 2F. PLoS One *12*, 1–23.
22. Khairani, A.F., Setiawan, C.J., Shanty, N., Lesmana, R., and Achadiyani, A. (2020). Molecular Mechanisms of Anthocyanins as A Potential Nutraceutical for Muscle Regeneration. Syst. Rev. Pharm. *11*, 189–202.
23. Saclier, M., Bonfanti, C., Antonini, S., Angelini, G., Mura, G., Zanaglio, F., Taglietti, V., Romanello, V., Sandri, M., Tonelli, C., et al. (2020). Nutritional intervention with cyanidin hinders the progression of muscular dystrophy. Cell Death Dis. *11*, 127.
24. Saclier, M., Lapi, M., Bonfanti, C., Rossi, G., Antonini, S., and Messina, G. (2020). The Transcription Factor Nfix Requires RhoA-ROCK1 Dependent Phagocytosis to Mediate Macrophage Skewing during Skeletal Muscle Regeneration. Cells *9*, 708.
25. King, A.J., Arnone, M.R., Bleam, M.R., Moss, K.G., Yang, J., Fedorowicz, K.E., Smitheman, K.N., Erhardt, J.A., Hughes-Earle, A., Kane-Carson, L.S., et al. (2013). Dabrafenib; Preclinical Characterization, Increased Efficacy when Combined with Trametinib, while BRAF/MEK Tool Combination Reduced Skin Lesions. PLoS One *8*, e67583.
26. Dumble, M., Crouthamel, M.C., Zhang, S.Y., Schaber, M., Levy, D., Robell, K., Liu, Q., Figueroa, D.J., Minthorn, E.A., Seefeld, M.A., et al. (2014). Discovery of novel AKT inhibitors with enhanced anti-tumor effects in combination with the MEK inhibitor. PLoS One *9*, e100880.
27. Qiu, J.G., Zhang, Y.J., Li, Y., Zhao, J.M., Zhang, W.J., Jiang, Q.W., Mei, X.L., Xue, Y.Q., Qin, W.M., Yang, Y., et al. (2015). Trametinib modulates cancer multidrug resistance by targeting ABCB1 transporter. Oncotarget *6*, 15494–15509.
28. Cowan, N., and Keiser, J. (2015). Repurposing of anticancer drugs: in vitro and in vivo activities against Schistosoma mansoni. Parasites Vectors *8*, 417.
29. Seale, P., Sabourin, L.A., Girgis-Gabardo, A., Mansouri, A., Gruss, P., and Rudnicki, M.A. (2000). Pax7 Is Required for the Specification of Myogenic Satellite Cells skeletal muscle are mitotically quiescent and are acti- vated in response to diverse stimuli, including stretch-ing, exercise, injury, and electrical stimulation (Schultz. Cell *102*, 777–786.
30. Seale, P., Ishibashi, J., Scimè, A., and Rudnicki, M.A. (2004). Pax7 is necessary and sufficient for the myogenic specification of CD45+:Sca1+ stem cells from injured muscle. PLoS Biol. *2*, E130.
31. Bencze, M., Periou, B., Baba-Amer, Y., and Authier, F.J. (2019). Immunolabelling Myofiber Degeneration in Muscle Biopsies. J. Vis. Exp. 154.
32. Forcina, L., Cosentino, M., and Musarò, A. (2020). Mechanisms Regulating Muscle Regeneration: Insights into the Interrelated and Time-Dependent Phases of Tissue Healing. Cells *9*.
33. Molina, T., Fabre, P., and Dumont, N.A. (2021). Fibro-adipogenic Progenitors in Skeletal Muscle Homeostasis, Regeneration and Diseases (Royal Society Publishing).
34. Chapman, V.M., Miller, D.R., Armstrong, D., and Caskey, C.T. (1989). Recovery of induced mutations for X chromosome-linked muscular dystrophy in mice. Proc. Natl. Acad. Sci. USA *86*, 1292–1296.
35. Li, C., Chen, Z., Yang, H., Luo, F., Chen, L., Cai, H., Li, Y., You, G., Long, D., Li, S., et al. (2016). Selumetinib, an oral anti-neoplastic drug, may attenuate cardiac hypertrophy via targeting the ERK pathway. PLoS One *11*, e01590799.
36. Quan-Jun, Y., Yan, H., Yong-Long, H., Li-Li, W., Jie, L., Jin-Lu, H., Jin, L., Peng-Guo, C., Run, G., and Cheng, G. (2017). Selumetinib attenuates skeletal muscle wasting in murine cachexia model through ERK inhibition and AKT activation. Mol. Cancer Therapeut. *16*, 334–343.
37. Young, C.N.J., Gosselin, M.R.F., Rumney, R., Oksiejuk, A., Chira, N., Bozycki, L., Matryba, P., Łukasiewicz, K., Kao, A.P., Dunlop, J., et al. (2020). Total Absence of Dystrophin Expression Exacerbates Ectopic Myofiber Calcification and Fibrosis and Alters Macrophage Infiltration Patterns. Am. J. Pathol. *190*, 190–205.
38. Angelini, G., Mura, G., and Messina, G. (2022). Therapeutic approaches to preserve the musculature in Duchenne Muscular Dystrophy: The importance of the secondary therapies. Exp. Cell Res. *410*, 112968.
39. Cheng, Y., and Tian, H. (2017). Current Development Status of MEK Inhibitors. Molecules *22*, 1551.
40. Shahid, S., Kushner, B.H., Modak, S., Basu, E.M., Rubin, E.M., Gundem, G., Papaemmanuil, E., and Roberts, S.S. (2021). Association of BRAF V600E mutations with vasoactive intestinal peptide syndrome in MYCN -amplified neuroblastoma. Pediatr. Blood Cancer *68*, e29265.
41. Voon, P.J., Chen, E.X., Chen, H.X., Lockhart, A.C., Sahebjam, S., Kelly, K., Vaishampayan, U.N., Subbiah, V., Razak, A.R., Renouf, D.J., et al. (2022). Phase I pharmacokinetic study of single agent trametinib in patients with advanced cancer and hepatic dysfunction. J. Exp. Clin. Cancer Res. *41*, 51.
42. Meyers, C., Lisiecki, J., Miller, S., Levin, A., Fayad, L., Ding, C., Sono, T., McCarthy, E., Levi, B., and James, A.W. (2019). Heterotopic Ossification: A Comprehensive Review. JBMR Plus *3*, e10172.
43. Moore-Lotridge, S.N., Li, Q., Gibson, B.H.Y., Martin, J.T., Hawley, G.D., Arnold, T.H., Saito, M., Tannouri, S., Schwartz, H.S., Gumina, R.J., et al. (2019). Trauma-Induced Nanohydroxyapatite Deposition in Skeletal Muscle is Sufficient to Drive Heterotopic Ossification. Calcif. Tissue Int. *104*, 411–425.
44. Kaplan, F.S., al Mukaddam, M., Stanley, A., Towler, O.W., and Shore, E.M. (2020). Fibrodysplasia ossificans progressiva (FOP): A disorder of osteochondrogenesis. Bone *140*, 115539.
45. Li, L., and Tuan, R.S. (2020). Mechanism of Traumatic Heterotopic Ossification: In Search of Injury-Induced Osteogenic Factors (Blackwell Publishing Inc).
46. Li, L., Jiang, Y., Lin, H., Shen, H., Sohn, J., Alexander, P.G., and Tuan, R.S. (2019). Muscle injury promotes heterotopic ossification by stimulating local bone morphogenetic protein-7 production. J. Orthop. Translat. *18*, 142–153.
47. van Putten, M., Putker, K., Overzier, M., Adamzek, W.A., Pasteuning-Vuhman, S., Plomp, J.J., and Aartsma-Rus, A. (2019). Natural disease history of the D2-mdx mouse model for Duchenne muscular dystrophy. FASEB (Fed. Am. Soc. Exp. Biol.) J. *33*, 8110–8124.
48. Giovannelli, G., Giacomazzi, G., Grosemans, H., and Sampaolesi, M. (2018). Morphological and functional analyses of skeletal muscles from an immunodeficient animal model of limb-girdle muscular dystrophy type 2E. Muscle Nerve *58*, 133–144.
49. Uezumi, A., Fukada, S.I., Yamamoto, N., Takeda, S., and Tsuchida, K. (2010). Mesenchymal progenitors distinct from satellite cells contribute to ectopic fat cell formation in skeletal muscle. Nat. Cell Biol. *12*, 143–152.
50. Mázala, D.A., Novak, J.S., Hogarth, M.W., Nearing, M., Adusumalli, P., Tully, C.B., Habib, N.F., Gordish-Dressman, H., Chen, Y.W., Jaiswal, J.K., and Partridge, T.A. (2020). TGF-β-driven muscle degeneration and failed regeneration underlie disease onset in a DMD mouse model. JCI Insight *5*, e135703.
51. Eisner, C., Cummings, M., Johnston, G., Tung, L.W., Groppa, E., Chang, C., and Rossi, F.M. (2020). Murine Tissue-Resident PDGFRα+ Fibro-Adipogenic Progenitors Spontaneously Acquire Osteogenic Phenotype in an Altered Inflammatory Environment. J. Bone Miner. Res. *35*, 1525–1534.
52. Lees-Shepard, J.B., Yamamoto, M., Biswas, A.A., Stoessel, S.J., Nicholas, S.A.E., Cogswell, C.A., Devarakonda, P.M., Schneider, M.J., Cummins, S.M., Legendre, N.P., et al. (2018). Activin-dependent signaling in fibro/adipogenic progenitors causes fibrodysplasia ossificans progressiva. Nat. Commun. *9*, 471.

53. Kassouf, T., and Sumara, G. (2020). Impact of conventional and atypical mapks on the development of metabolic diseases. Biomolecules *10*, 1256–1334.

54. Sun, Y.M., Qin, J., Liu, S.G., Cai, R., Chen, X.C., Wang, X.M., and Pang, W.J. (2017). PDGFRα regulated by miR-34a and FoxO1 Promotes adipogenesis in porcine intramuscular preadipocytes through erk signaling pathway. Int. J. Mol. Sci. *18*, 2424.

55. Kyono, A., Avishai, N., Ouyang, Z., Landreth, G.E., and Murakami, S. (2012). FGF and ERK signaling coordinately regulate mineralizationrelated genes and play essential roles in osteocyte differentiation. J. Bone Miner. Metabol. *30*, 19–30.

56. Mignemi, N.A., Yuasa, M., Baker, C.E., Moore, S.N., Ihejirika, R.C., Oelsner, W.K., Wallace, C.S., Yoshii, T., Okawa, A., Revenko, A.S., et al. (2017). Plasmin Prevents Dystrophic Calcification After Muscle Injury. J. Bone Miner. Res. *32*, 294–308.

57. Nutter, F.H., Haylor, J.L., and Khwaja, A. (2015). Inhibiting ERK Activation with CI-1040 Leads to Compensatory Upregulation of Alternate MAPKs and Plasminogen Activator Inhibitor-1 following Subtotal Nephrectomy with No Impact on Kidney Fibrosis. PLoS One *10*, e0137321.

58. Jablonski, K.L., and Chonchol, M. (2013). Vascular calcification in end-stage renal disease. Hemodial. Int. *17* (*Suppl 1*), S17–S21.

59. Ranganathan, K., Loder, S., Agarwal, S., Wong, V.W., Forsberg, J., Davis, T.A., Wang, S., James, A.W., and Levi, B. (2015). Heterotopic Ossification: Basic-Science Principles and Clinical Correlates. J. Bone Joint Surg. Am. *97*, 1101–1111.

60. Hawellek, T., Hubert, J., Hischke, S., Vettorazzi, E., Wegscheider, K., Bertrand, J., Pap, T., Krause, M., Püschel, K., Rüther, W., and Niemeier, A. (2016). Articular cartilage calcification of the humeral head is highly prevalent and associated with osteoarthritis in the general population. J. Orthop. Res. *34*, 1984–1990.

61. Muchir, A., Kim, Y.J., Reilly, S.A., Wu, W., Choi, J.C., and Worman, H.J. (2013). Inhibition of extracellular signal-regulated kinase 1/2 signaling has beneficial effects on skeletal muscle in a mouse model of Emery-Dreifuss muscular dystrophy caused by lamin A/C gene mutation. Skeletal Muscle *3*, 17.

62. Heller, S.A., Shih, R., Kalra, R., and Kang, P.B. (2020). Emery-Dreifuss muscular dystrophy. Muscle Nerve *61*, 436–448.

63. Wang, C., and Wang, K. (2019). Rapid screening of CRISPR/Cas9-induced mutants using the ACT-PCR method. In Methods in Molecular Biology (Humana Press Inc), pp. 27–32.

64. Boyer, J.G., Huo, J., Han, S., Havens, J.R., Prasad, V., Lin, B.L., Kass, D.A., Song, T., Sadayappan, S., Khairallah, R.J., et al. (2022). Depletion of skeletal muscle satellite cells attenuates pathology in muscular dystrophy. Nat. Commun. *13*, 2940.

65. Petroni, K., Trinei, M., Fornari, M., Calvenzani, V., Marinelli, A., Micheli, L.A., Pilu, R., Matros, A., Mock, H.-P., Tonelli, C., and Giorgio, M. (2017). Dietary cyanidin 3-glucoside from purple corn ameliorates doxorubicin-induced cardiotoxicity in mice. Nutr. Metabol. Cardiovasc. Dis. *27*, 462–469.

66. Sambasivan, R., Yao, R., Kissenpfennig, A., Van Wittenberghe, L., Paldi, A., Gayraud-Morel, B., Guenou, H., Malissen, B., Tajbakhsh, S., and Galy, A. (2011). Pax7-expressing satellite cells are indispensable for adult skeletal muscle regeneration. Preprint *138*, 4333.

67. Desgeorges, T., Liot, S., Lyon, S., Bouvière, J., Kemmel, A., Trignol, A., Rousseau, D., Chapuis, B., Gondin, J., Mounier, R., et al. (2019). Open-CSAM, a new tool for semi-automated analysis of myofiber cross-sectional area in regenerating adult skeletal muscle. Skeletal Muscle *9*, 2.

STAR★METHODS

KEY RESOURCES TABLE

REAGENT or RESOURCE	SOURCE	IDENTIFIER
Antibodies		
Rabbit polyclonal anti-Nfix	Geneka	Cat# 16021118
Rabbit polyclonal anti-Nfix	Novus Biological	Cat# NBP2-15038; RRID:AB_2891313
Monoclonal polyclonal anti-Vinculin	Sigma-Aldrich	Cat# V9131; RRID:AB_477629
Rabbit polyclonal anti-p44/42 MAPK (Erk1/2) (Thr202/Tyr204)	Cell Signaling	Cat# 9101; RRID:AB_331646
Rabbit polyclonal anti-p44/42 MAPK (Erk1/2)	Cell Signaling	Cat# 9102; RRID:AB_330744
Goat Anti-Mouse IgG (H + L)-HRP Conjugate	Bio-Rad	Cat# 1706516; RRID:AB_2921252
Goat Anti-Rabbit IgG (H + L)-HRP Conjugate	Bio-Rad	Cat# 1706515; RRID:AB_11125142
Rat polyclonal anti-Laminin	Invitrogen	Cat# MA1-06100; RRID:AB_559896
Goat polyclonal anti-Collagen I	Southern Biotech	Cat# 131001; RRID:AB_609609
Rat polyclonal anti-F4/80	Novus Biological	Cat# NB 600-404; RRID:AB_350686
Goat polyclonal anti-PDGFRα	RD Systems	Cat# AF1062
Mouse monoclonal anti-totMyHC	Dev Studies Hybridoma Bank	Cat# MF20; RRID:AB_2147781
IgG Goat anti-Mouse Alexa Fluor 594 nm	Thermofisher	Cat# A11032; RRID:AB_2534091
IgG Goat anti-Rabbit Alexa Fluor 488 nm	Thermofisher	Cat# A11008; RRID:AB_143165
IgG Rat anti-Mouse Alexa Fluor 647 nm	Thermofisher	Cat# A21247; RRID:AB_141778
IgG Donkey anti-Rabbit Alexa Fluor 488 nm	Thermofisher	Cat# A21206; RRID:AB_2535792
IgG Donkey anti-Goat Alexa Fluor 594 nm	Thermofisher	Cat# A11058; RRID:AB_2313737
IgG Donkey anti-Goat Alexa Fluor 488 nm	Thermofisher	Cat# A11055; RRID:AB_2534102
IgG Rat anti-Goat Alexa Fluor 594 nm	Thermofisher	Cat# A11007; RRID:AB_10561522
Biological samples		
Murine skeletal muscles	This paper	N/A
Chemicals, peptides, and recombinant proteins		
Trametinib (Mekinist)	Selleckchem	Cat# GSK1120212
Selumetinib (AZD6244)	Selleckchem	Cat# S1008
Cyanidin-3-glucoside powder	This paper	N/A
Cardiotoxin	Latoxan	Cat# L8102
Critical commercial assays		
DC Protein Assay	Bio-Rad	Cat# 5000116
SYBR Green Supermix	Bio-Rad	Cat# 1725274
Experimental models: Organisms/strains		
Mouse: CD-1	Charles River	Crl:CD1(ICR)
Mouse: C57BL/6J:WT	Charles River	C57BL/6NCrl
Mouse: C57BL/6J:*Sgca* null	Laboratory of Giulio Cossu	N/A
Mouse: C57BL/6J:*mdx4cV*	Laboratory of Giulio Cossu	N/A
Oligonucleotides		
Nfix fwd: CACTGGGGCGACTTGTAGAG	Eurofins Genomics	N/A
Nfix rev: AGGCTGACAAGGTGTGGC	Eurofins Genomics	N/A
β-actin fwd: CTCTGGCTCCTAGCACCATGAAGA	Eurofins Genomics	N/A
β-actin rev: GTAAAACGCAGCTCAGTAACAGTCCG	Eurofins Genomics	N/A

(*Continued on next page*)

Continued

REAGENT or RESOURCE	SOURCE	IDENTIFIER
INT1 alpha (*Sgca* null genotyping): CAGGGCTGGGAGCTGGGTTCTG	Eurofins Genomics	N/A
EX2 alpha (*Sgca* null genotyping): CCCAGGGCCTTGATGCCT	Eurofins Genomics	N/A
MepTR alpha (*Sgca* null genotyping): CCCAGGGCCTTGATGCCT	Eurofins Genomics	N/A
Common Rev (*mdx* genotyping): GCGCGGCTTGCCTCTGACCTGTCCTAT	Eurofins Genomics	N/A
Wild type Fw (*mdx* genotyping): GCGCGGCTTGCCTCTGACCTGTCCTAT	Eurofins Genomics	N/A
Other		
Hematoxylin	Sigma Aldrich	Cat# HHS32
Eosin	Sigma Aldrich	Cat# E4382
Alizarin Red S	Sigma Aldrich	Cat# A5533
Oil Red O	Sigma Aldrich	Cat# 01391

RESOURCE AVAILABILITY

Lead contact

Further information and requests for resources and reagents should be directed to and will be fulfilled by the lead contact, Graziella Messina (graziella.messina@unimi.it).

Materials availability

This study did not generate new unique reagents.

Data and code availability

- This study did not generate any unique datasets or code.
- Any additional information required to reanalyze the data reported in this paper is available from the lead contact upon request.

EXPERIMENTAL MODEL AND STUDY PARTICIPANT DETAILS

Wildtype C57BL/6J, Sgca null, and mdx mice

In this study we used 6-week-old WT mice of C57BL/6J background and, as dystrophic counterparts, the *Sgca* null mice[20] and the *mdx* mouse model[34] of both sexes, randomly assigned to experimental groups, for the *in vivo* experiments. All mice were maintained under pathogen-free conditions with 12 h/12 h light/dark cycles. Mice undergoing different treatments, concerning both drug administration and liquid supplementation, were housed in different ventilated cages. Food and water were supplied *ad libitum*. Body weight was monitored daily during drug administration. All the experimental procedures were carried out in accordance with the Italian law (D. Lgs n. 2014/26, implementation of 2010/63/UE) and approved by the University of Milan Animal Welfare Body and by the Italian Health Ministry.

Wildtype CD1 mice, primary myoblasts and fibroblasts

Juvenile MuSC-derived myoblasts were isolated from 10-day-old WT murine pups. All hindlimb muscles were collected from each mouse and placed into DF50 medium (Dulbecco's Modified Eagle Medium, 50% Fetal Bovine Serum Gibco 10270-106, 1% Penicillin/Streptomycin Euroclone ECB3001D). Non-muscular tissues were removed by a stereomicroscope in sterile conditions. Muscles were mechanically and enzymatically digested for 20 min at 37°C under strong agitation with 1.5 mg/mL Dispase (Gibco 17105041), 0.15 mg/mL Collagenase (Sigma C9263), and 0.1 mg/mL DNase I (Roche 11284932001) in PBS 1X (EuroClone ECB4004L). After every digestion cycle, dissociated cells were collected in DF10 medium (DMEM, 10% FBS, 1% P/S, 1% L-Glutamine EuroClone ECB30000D) at 4°C to inactivate the enzymes. Once all the digestion cycles have finished and all cells have been gathered in the same tubes, they were centrifuged at 300 g for 5 min at 4°C. The pellet was resuspended in DF10 medium and filtered using the 70-μm nylon filter and then the 40-μm nylon filter. Filtered cells were centrifuged at 300 g for 5 min at 4°C, and the supernatant was discarded.

Cell pellet was resuspended in MACS Buffer (phosphate-buffered saline, pH 7.2, 0.5% bovine serum albumin, 2 mM EDTA) and Satellite Cell Isolation Kit (Miltenyi Biotec, 130-104-268) according to manufacturer instructions. The mixture was incubated at 4°C, for 15 min and then magnetically separated following the Miltenyi protocol. The flow-through, which contains the myogenic cells, was collected, centrifuged at 300 g for 5 min, and resuspended in proliferation medium for satellite cells (DMEM, 20% FBS, 10% Horse Serum Euroclone ECS0090L, 1% P/S, 1% L-Glutamine, 0.1% Gentamycin Sigma G1397, 2.5 ng/mL β-FGF Peprotech 100-18B).

Cells were plated on collagen-coated dishes at ~500 cells/cm^2 (Collagen from calf skin, Sigma, C9791) and incubated at 37°C, 5% CO2 for 48 h. The proliferation medium was completely replaced after 24 h. After that, cells were washed twice with Dulbecco's Phosphate Buffered Saline 1X (PBS, EuroClone ECB4004L). 1 mL of diluted Trypsin (1:1 with PBS 1X, Sigma T4174) was added to allow detachment of MuSC-derived myoblasts. The cells were incubated for 1–2 min at 37°C, 5% CO2. The trypsinization was then quickly blocked by addition of 5 mL of FBS-containing medium, which were used to collect all the cells. The gathered cells were then centrifuged at 300 g for 5 min, the pellet was resuspended in an adequate volume of proliferation medium, and then plated in collagen-coated dishes at ~5000 cells/cm^2 in proliferation medium and incubated at 37°C, 5% CO2.

After the incubation with diluted Trypsin, primary fibroblasts were still attached to the dishes. After some days in culture with DF10 medium, fibroblasts were incubated with Trypsin for 5 min at 37°C, 5% CO2 to allow detachment of cells, gathered in DF10 medium and then plated at ~7000 cells/cm^2 into plastic dishes for 1 h, 37°C, 5% CO2. After that, supernatant medium was removed, changed with fresh DF10 medium and let fibroblasts grow for 2 days, ready to be treated.

Concerning the differentiation experiment, MuSC-derived myoblasts were seeded at 200000 cells/cm^2 onto collagen-coated petri dishes. The next day, cells were treated with DMSO or Trametinib for 16 h and then proliferation medium was replaced with differentiation medium (DMEM, 5% Horse Serum, 1% P/S, 1% L-Glutamine). At 4th days of differentiation, myotubes were stopped to be analyzed.

Primary macrophage cell culture

Total mouse bone marrow was obtained by flushing femur and tibiae with DMEM and cells were cultured in DMEM containing 20% Fetal Bovine Serum (FBS) and 30% of L929 cell line-derived conditioned medium (enriched in CSF-1) for 6–7 days. MPs were polarized toward M2 status using 10 ng/mL IL10 (Peprotech #210-10) in DMEM containing 10% FBS for 2 days.

METHOD DETAILS

Drug treatment *in vitro*

PD98059 (Cell signaling, 9900) were dissolved in dimethyl sulfoxide (DMSO, Sigma, 20–139) and added to myoblasts at 50 μM, respectively, for 16 h, at 37°C, 5% CO2.

Trametinib (GSK1120212, Mekinist) was purchased from Selleckchem and dissolved in DMSO at stock dilutions of 12 mg/mL under sterile conditions; then, it was added at different concentrations to the growth medium of juvenile MuSC-derived myoblasts, for 16 h. For each experimental condition, cells treated with 0.1% DMSO were used as control.

After the treatment, the cells allocated for molecular biology studies (protein or RNA extraction) were washed twice with cold PBS 1X and frozen at −20°C. For immunofluorescence assays, cells were briefly washed with PBS 1X at room temperature and immediately fixed (see immunofluorescence protocol).

Treatment with MEK-inhibitors *in vivo*

Selumetinib (AZD6244, S1008) was purchased from Selleckchem and dissolved in DMSO at stock dilutions of 30 mg/mL under sterile conditions.

Working dilutions of Trametinib and Selumetinib were dissolved at a dose volume of 0.2 mL/20 g body weight in 0.5% hydroxypropylmethylcellulose (Sigma-Aldrich H7509), 0.2% Tween-80 (Sigma-Aldrich P1754) in distilled water (pH 8.0). Adult mice were treated at specific concentrations of Trametinib or Selumetinib by oral gavage (plastic feeding tubes, 20ga x 38 mm, Instech, FTP-20-38-50), every day for 14 days, and then sacrificed at 4 h post dose. Control mice were treated with vehicle only (DMSO).

Cyanidin-enriched diet

Cyanidin-3-glucoside powder was synthetized by the Laboratory of Prof. K. Pertroni from a novel anthocyanin-rich hybrid maize carrying the B1 and Pl1 alleles, which confer anthocyanin pigmentation in seed pericarp and all plant tissues.[65] Cyanidin powder was dissolved in acidified water (pH: 3.5–3.8 with HCl) to a final concentration of 7.7 mg/mL and administered *ad libitum* to animals from 3 to 8 weeks of age in feeding bottle protected from light. Liquid Cyanidin in feeding bottle was changed every two days, monitoring the level of liquid consumption.

Grip strength test

Muscular functionality was measured by the grip strength test, which assess the force generated by each mouse grasping a grid connected to a dynamometer. From three to five trials with front and hind paws combined were independently performed for each mouse. The data were normalized to the animal weight. The average force for each treatment group was expressed in milli Newton (mN) and graphed as a measure of grip strength.

Forced downhill strenuous exercise

We followed the protocol of strenuous resistance exercise described by Sambasivan and colleagues[66]: forward-moving belt (Bioseb, Vitrolles, France) set at 12 m/min with a declining slope of 30° for the first day and 15° for days 2–5, for 30 min per day for the last 5 days of Trametinib treatment.

Protein extraction and western blotting

Protein extracts were obtained from cultured cells lysed with RIPA buffer (10 mM Tris-HCl pH 8.0, 1 mM EDTA, 1% Triton X-, 0.1% sodium deoxycholate, 0.1% SDS, 150 mM NaCl in deionized water) for 30 min on ice, while total protein extracts from adult muscles were obtained from homogenized tissues in Tissue extraction buffer (50 mM Tris-HCl, 1 mM EDTA, 1% Triton X-, 150 mM NaCl). Protease and phosphatase inhibitors were always added to both RIPA and Tissue extraction Buffer. After lysis, samples were centrifugated at 10000 g, 4°C, 10 min and the supernatants were collected and quantified using the DC Protein Assay (Bio-Rad, 5000116).

40 μg of total protein extract was denatured with SDS Page Loading sample buffer (100 mM Tris pH 6.8, 4% SDS, 0.2% Bromophenol blue, 20% Glycerol and 10 mM dithiothreitol) and heated at 95°C for 5 min. Then, denatured protein samples were loaded on 8–10% SDS acrylamide gel to perform electrophoresis running and then blotted to nitrocellulose transfer membrane 0.45 μm (ThermoScientific, 88018). Afterward, the membrane was blocked in 5% Milk in TBST 1X (NaCl 150 mM, Tris-HCl 20 mM, Tween 20 0.02%) for 1 h and then primary antibodies dissolved in 5% Milk TBST 1X or Signal Boost (Calbiochem 407207) were incubated O/N at 4°C in agitation. We used the following primary antibodies and dilutions: rabbit anti-Nfix (1:2500, Geneka, 16021118), mouse anti-Vinculin (1:2500, Sigma-Aldrich, V9131), rabbit anti-pERK 1,2 (1:1000, Cell Signaling, 9101), rabbit anti-ERK 1,2 (1:1000, Cell Signaling, 9102). The day after, blots were washed with TBST 1X and incubated with secondary antibodies (1:10000, anti-mouse or anti-rabbit, IgG-HRP, Bio-Rad, 1706516, 1706515) at room temperature for 45 min in 5% Milk TBST 1X. Protein bands were revealed through ECL detection reagent (GeneSpin, PDS standard) and images were acquired using the ChemiDoc MP System (Bio-Rad). The Image Lab software was used to measure and quantify the bands of independent Western blot experiments. The obtained absolute quantity was compared with the reference band and expressed in the graphs as normalized volume (Norm. Vol. Int.). All the values are presented as mean ± sem.

RNA extraction and qRT-PCR

Total RNA was isolated from muscle sections or myogenic cells through the TRIzol Reagent protocol (Invitrogen, 15596026). The obtained RNA pellet was let air dry for about 10 min avoiding its complete dryness and then resuspended in 10–15 μL of Nuclease-free water (Thermofisher, 4387936). RNA samples were quantified through NanoDrop Spectrophotometer (Implen) and stored at −80°C or retrotranscribed.

Total RNA was retrotranscribed to complementary DNA (cDNA) with iScript Reverse Transcription Supermix (Bio-Rad, 1708840) following the manufacturer protocol.

The cDNA obtained was diluted in RNase-free water and stored at −20°C or used for qRT-PCR. The real-time PCR was performed using SYBR Green Supermix (Bio-Rad, 1725274). Relative mRNA expression levels were normalised on the *β-actin* gene expression levels.

We used the following primers: *Nfix* fwd CACTGGGGCGACTTGTAGAG; *Nfix* rev AGGCTGACAAGGTGTGGC; *β-actin* fwd CTCTGGC TCCTAGCACCATGAAGA; *β-actin* rev GTAAAACGCAGCTCAGTAACAGTCCG.

Inclusion and cryo-sectioning of muscles

Left and right *Tibialis anterior*, *Soleus*, *Gastrocnemius* and Diaphragm muscles were collected from each mouse and vertically placed on a cork support with a small amount of inclusion gum (Tragacanth Gum Sigma, G1128). Then, muscles were put in Isopentane (Carlo Erba, 524391), which was precooled in liquid nitrogen. After 2–5 min in isopentane, muscles were immersed in liquid nitrogen and conserved at −80°C.

Muscles were serially cut with the cryostat (Leica, CM1850) at −25°C. The width of each muscle slice was fixed at 7 μm, and they were collected on Super frost Microscope slides (Thermo-Fisher Scientific, 10123560WCUT). For each muscle, representative transverse sections were collected.

Immunofluorescence

For IF on Laminin, IgG, Nfix, Collagen I and tot MyHC, muscle slides or cells received fixation with PFA 4% for 15 min at room temperature, followed by 2 washes in PBS 1X (Sigma Aldrich, P4417). Hereafter, all immunostainings were performed following the same protocol. Muscles were permeabilized with a solution of 0.2% Triton X-100 (Sigma Aldrich, T8787), 1% Bovine Serum Albumin (BSA, Gene Spin, STS-BSA 100) in PBS 1X for 30 min at RT. Thereafter, sections were blocked with Goat Serum 10% (Sigma Aldrich, G9023) in PBS 1X for 30 min at room temperature and incubated with primary antibodies diluted in Goat Serum 1,5% or BSA 1% in PBS 1X, O/N at 4°C in humidity chamber and in the dark. In this study, we used the following primary antibodies: anti-Laminin antibody (1:300, Rat, Invitrogen, MA1-06100), anti-Collagen Type I antibody (1:500, Goat, Southern Biotech, 1310-01), anti-F4/80 antibody (1:400, Rat, Novus Biological, NB600-404), anti-PDGFRα antibody (1:500, Goat, RD Systems, AF 1062), anti-Nfix antibody (1:200, Rabbit, Novus Biological, NBP2-15038), anti-totMyHC (1:1, Mouse Hybridoma, Developmental Studies Hybridoma Bank). The day after, slides were washed with a solution of 0.2% Triton X-100, 1% BSA in PBS 1X for 5 and 15 min at room temperature and incubated for 45 min in darkness with a pre-centrifugated (5 min, 6000 g) solution containing secondary antibodies and Hoechst (1: 500, Sigma-Aldrich B2261) diluted in PBS 1X. We used the following secondary antibodies: IgG Goat anti-Mouse Alexa Fluor 594 nm (1:250, Thermofisher, A-11032), IgG Goat anti-Rabbit Alexa Fluor 488 nm (1:250, Thermofisher, A-11008), IgG Goat anti- Alexa Fluor Rat 647 nm (1:250, Thermofisher, A-21247), IgG Donkey anti-Rabbit Alexa Fluor 488 nm (1:250, Thermofisher, A-21206), IgG Donkey anti-Goat Alexa Fluor 594 nm (1:250, Thermofisher, A-11058), IgG Donkey anti-Goat Alexa Fluor 488 nm (1:250, Thermofisher, A-11055), IgG Goat anti-Rat Alexa Fluor 594 nm (1:250, Thermofisher, A-11007).

After 2 washes in 0.2% Triton X-100 in PBS 1X solution for 5 and 15 min, slides were cleaned in distilled water for 5 min then mounted with Fluoromount Plus (Diagnostic BioSystems K048) and covering glasses. Slides were acquired at fluorescent microscope soon after drying of mounting medium, then stored at 4°C in darkness.

Hematoxylin & eosin staining

Muscle slides were dipped in distilled water for 1 min, then stained with Hematoxylin of Meyer (Sigma, HHS32) for 4 min in the dark. Subsequently, muscle sections were rinsed in distilled water and put under running water for at least 15 min. Next, slides were rinsed again in distilled water and dehydrated in enthanol 70% for 1 min and in ethanol 90% for 2 min. Then, sections were stained in a solution of 0,5% eosin (Sigma, E4382) in ethanol, in the dark for 7 min. Subsequently, slides were dehydrated with passages in ethanol 90% for 1 min, 95% for 2 min and 100% for 5 min. Finally, sections were cleaned in xylene, and mounted with clover glasses and Eukitt mounting medium (Bio Optica, 09–00250). They were let dry overnight under a chemical hood and conserved at room temperature protected from the sunlight.

Alizarin Red staining

Slices were thawed at room temperature and directly dipped in Alizarin Red S (Sigma Aldrich, A5533-25G) for 4 min, then rinsed abundantly in distilled water to remove the excess of coloration. Slices were passed from Acetone 100% to Acetone/Xylene 1:1 solution for at least 35 s each. Therefore, after 2 passages in Xylene 100% for at least 45 s, slides were mounted with cover glasses and Eukitt (Bio-optica, W01030706), dried overnight under chemical hood and stored at room temperature in the dark.

Oil Red O staining

Muscle slices were thawed at room temperature and directly dipped in 2-propanol 60% for 20 s, then rinsed into 1:1.5 Oil Red O solution (Sigma Aldrich, 01391) for 10 min, and again in 2-propanol 60% for 30 s. Slices were passed in distilled water to remove the excess of coloration for 20 s and then under running tap water for 3 min. Slides were mounted with cover glasses and aqueous mounting solution.

Cross-sectional area and myotube length

Images of stained muscle slices were acquired by nanozoomer S60 (Hamamatsu) of Unitech NoLimits facility at University of Milan. Images of IF were acquired by the inverted microscope (Leica-DMI6000B) equipped with Leica DFC365FX and DFC400 cameras and ×10, ×20, ×40 magnification objectives. The Leica Application Suite software was used for acquisition.

The cross-sectional area (CSA) of myofibers was evaluated on anti-Laminin immunofluorescent staining of *Tibialis anterior* and Diaphragm muscle sections. Images of the entire section were split into two-half and separately analyzed with the Open-CSAM tool of the ImageJ software.[67] The ImageJ software was used to calculate the average myotube length *in vitro*.

QUANTIFICATION AND STATISTICAL ANALYSIS

All data are expressed as mean ± SEM. Graphs were obtained using GraphPad Prism software and analyzed with Normalization test and the appropriate statistical test, as indicated in figure legends together with sample size. We used two-tailed t-test or one-way ANOVA to compare two groups or more than two sets, respectively. *$p < 0.05$, **$p < 0.01$, ***$p < 0.001$, confidence interval 95%, alpha level 0.05.